Evolutionary Diversity of the Mitochondrial Calcium Uniporter and Its Contribution to Cardiac and Vascular Homeostasis

Abstract

Altered cardiac energetics and calcium handling are characteristic features of cardiovascular disease. Mitochondria play a significant role in both cellular energy generation and calcium homeostasis and may be a key integration point of these two systems. Calcium uptake into mitochondria occurs via a recently identified mitochondrial calcium uniporter complex.

In the first part of this thesis, I characterize the phylogenomic distribution of the uniporter's membrane spanning pore (MCU) and regulatory subunits (MICU1 and MICU2). Homologs of both MCU and MICU1 tend to co-occur in all major branches of eukaryotic life but both have been lost along certain protozoan and fungal lineages. MICU2 represents a recent duplication of MICU1. Several bacterial genomes also contain putative MCU homologs that may represent prokaryotic calcium channels. The analyses indicate that the uniporter may have been an early feature of mitochondria.

In the second part of this thesis, I perform transcriptome wide analysis of human and mouse cardiomyopathy datasets and identify *MICU2*, a regulatory component of the mitochondrial calcium uniporter, as one of six genes consistently upregulated in cardiac disease states. I test the hypothesis that increased *MICU2* expression is cardio-protective by generating a global *Micu2*$^{-/-}$ mouse. These mice have diastolic dysfunction. Isolated *Micu2*$^{-/-}$ cardiomyocytes show altered sarcomere relaxation and cytosolic calcium reuptake kinetics and *Micu2*$^{-/-}$ ventricular tissue has transcriptional dysregulation of genes encoding sarcomere proteins and bZIP transcription factors. When exposed to two weeks of angiotensin 2, a pharmacologic hypertrophic stimuli, *Micu2*$^{-/-}$ mice exhibit both systolic and diastolic dysfunction.

Additionally, ~30% of *Micu2*$^{-/-}$ mice exposed to angiotensin 2 died within the first week from abdominal aortic rupture. The increase in abdominal aortic diameter is angiotensin 2 dose dependent. Norepinephrine treatment does not cause abdominal aorta dilatation, suggesting an angiotensin 2 specific effect rather than a blood pressure mediated effect. Transcriptional profiling of angiotensin treated Micu2$^{-/-}$ aortas show evidence of extracellular matrix remodeling due to matrix metaloprotease activity. Single-cell RNA-seq of aorta treated with angiotensin 2 identified differential expression of reactive oxygen species, inflammation and proliferation genes in fibroblast and smooth muscle cells, suggesting an early mechanism triggering aneurism formation. Together, these data point to a significant and previously unappreciated role for *Micu2* in maintaining both cardiac and vascular homeostasis.

Table of Contents

Glossary

CVD: Cardiovascular disease

HCM: Hypertrophic cardiomyopathy

DCM: Dilated cardiomyopathy

MCU: Mitochondrial Calcium Uniporter

MICU1: Mitochondrial calcium uptake protein 1

MICU2: Mitochondrial calcium uptake protein 2

Acknowledgments

I would like to dedicate this thesis to the many people who have guided me through my medical studies. First and foremost, I am tremendously grateful for the support and mentorship of my MD thesis research advisors Jonathan Seidman, Christine Seidman and Vamsi Mootha. Their keen interest in in my success has been unwavering. Their dual enthusiasm for scientific inquiry and medicine is infectious.

I thank the countless members of the Harvard Medical School Faculty who have guided me in my development as a physician-scientist in both the pre-clinical courses and as a developing clinician on the hospital wards. I would especially like to acknowledge the Harvard-MIT Health Sciences and Technology program faculty and Harvard-MIT MD/PhD program faculty for the opportunity to pursue this course of study. I also thank the National Institutes of Health National Heart, Lung and Blood Institute, the Leducq Foundation, and the Howard Hughes Medical Institute for financial support.

I have been aided immensely by the knowledge and kindness of many members of the Seidman and Mootha laboratories, without whom I could not have completed this work. Lastly, I am grateful beyond measure for my wife Sarah and my entire family for their unbounded love and devotion.

Collaborative Research Statement

The research presented in this thesis is derived from two manuscripts:

Bick AG, Calvo SE, Mootha VK. Evolutionary diversity of the mitochondrial calcium uniporter. Science. 2012; 336(6083):886. doi:10.1126/science.1214977. PubMed PMID: 22605770.

Bick AG, Wakimoto H, Kamer KJ, Sancak Y, Goldberger O, Axelsson A, DeLaughter DM, Gorham J, Mootha VK, Seidman JG, Seidman CE. Cardiac and vascular homeostasis dependent on MICU2, a regulatory subunit of the mitochondrial calcium uniporter. *In review*.

In both manuscripts, I conceived of the research project in discussions with Drs. Mootha, J. Seidman and C. Seidman, performed the majority of the experiments, was principally responsible for data analysis and production of the figures and wrote the first draft of the text which was subsequently revised with input from all authors. Figures 1 and 2 of this thesis are reproduced from the first manuscript (Bick, Science 2012) and Figures 3-9 and all tables are derived from the second manuscript (Bick, *In review*).

Introduction

Cardiovascular disease, heart failure and cardiomyopathy

Cardiovascular disease (CVD) is the leading cause of death in the United States and is responsible for 17% of national health expenditures (1). Although cardiovascular disease comes in many forms, a significant proportion of this disease burden is due to heart failure, a complex clinical syndrome that results from any structural or functional impairment of ventricular filling or ejection of blood (2). The lifetime risk of developing heart failure is 20% for Americans over the age of 40 and increases with age, thus the burden of disease is expected to grow significantly in the coming decades (3, 4). The total cost of heart failure associated healthcare in the United States exceeds $30 billion annually, or approximately 1% of all US healthcare spending (5).

The majority of heart failure is associated with cardiomyopathies a heterogeneous group of diseases of the cardiac muscle associated with mechanical dysfunction that result in inappropriate ventricular hypertrophy (HCM) or dilatation (DCM) (6-8). While the two disease entities are quite distinct in terms of natural history, both HCM and DCM may be caused by mutations in the genes that encode the protein constituents of the cardiac sarcomere, the contractile apparatus of the cardiac myocytes (9). Despite our increasingly complete enumeration of mutations that cause cardiomyopathy, progress elucidating mechanisms amenable to therapeutic intervention has been more limited (10).

Altered Cellular Energetics and Calcium Signaling Cause Cardiomyopathy

Work over the past 50 years demonstrates that altered cardiac energetics is the mechanistic cause of cardiomyopathy (11-13). Sarcomere protein gene mutations, the most common genetic cause of HCM and DCM, alters cardiomyocyte excitation/contraction coupling, which directly or indirectly results in altered cardiomyocyte energetics (14-17). One leading hypothesis is that changes in sarcomere function leads to cellular calcium fluxes, which in turn alters the balance of energy utilization and production in an individual cardiomyocyte (18, 19). The myocyte adapts to this change in energy homeostasis by reactivating fetal gene programs as well as

inducing fibrosis and maladaptive cardiac remodeling which results in cardiac remodeling (20, 21).

Directly altering cardiomyocyte energetics, as is often the case in patients with mitochondrial disease, also causes cardiomyopathy (22). Notably, cardiac muscle disease is a common feature of patients with maternally inherited mitochondrial disorders such as MELAS and MERRF (23), as well as in patients with Mendelian disorders of oxidative phosphorylation, including those due to mutations in *TMEM70* (24), AGK (25) and AARS2 (26). Outside of the cardiovascular system, altered cellular energetics in patients with mitochondrial disease commonly cause a range of disease phenotypes including diabetes, neurological disease, vision loss, and deafness (22). Less commonly, patients with mitochondrial disease have been described with aortic dilation (27) and aortic rupture (28).

Mitochondria Integrate Cellular Energetics and Calcium Homeostasis

Mitochondria are a primary source of energy in eukaryotic cells, but also play a major role in diverse cellular metabolic and homeostatic processes. Mitochondria have an endosymbiotic origin and retain many features of their proto-bacterial ancestor, including a double membrane and a circular genome. They also resemble bacteria in that they are typically about one micron in length and constantly move, divide and fuse to form a dynamic network (29). The majority of what was once the proto-mitochondrial genome has been transferred to the eukaryotic nuclear genome over billions of years of co-evolution. Of the ~1,000 mitochondrial proteins, about two-thirds have bacterial origins from multiple bacterial phyla. (30).

Mitochondria generate energy through the respiratory chain which enables oxidative phosphorylation. The respiratory chain consists of four complexes that catalyze electron transfer from reducing equivalents to molecular oxygen. Free energy is conserved by coupling electron transport to the formation of a proton gradient, or proton motive force, by three of these complexes (I, III and IV), which is then dissipated by F_1F_0-ATPase (complex V) for ATP synthesis (31). Many biochemical processes are coupled to the proton motive force including NADPH generation through nicotinamide nucleotide transhydrogenase (32), ATP/ADP exchange through the adenine nucleotide

translocator (33), protein import through the translocase of the inner mitochondrial membrane (34), inorganic phosphate transport (35) and calcium transport (36).

Mitochondria from different organs exhibit distinct patterns of fuel use and biosynthetic capacities. For example, adrenal mitochondria are capable of high capacity steroid hormone biosynthesis, while skeletal-muscle mitochondria specialize in fatty acid oxidation (29). Even within individual cells, mitochondria exhibit marked heterogeneity: intermyofibrillar and subsarcolemmal mitochondria have distinct fuel preferences and differential responses to stress in both skeletal muscle and cardiac muscle (37, 38).

Given the significant energy requirements of cardiac muscle it is unsurprising that tight coupling exists between cardiomyocyte and mitochondria (39, 40). Much of this coupling is thought to be mediated by calcium (41).

The Mitochondrial Calcium Uniporter

One remarkable feature of vertebrate mitochondria is their ability to uptake and buffer large amounts of calcium via a channel called the mitochondrial calcium uniporter. Its activity was first documented 50 years ago when two groups simultaneously discovered that mitochondria take up and buffer large amounts of calcium when treated with phosphate (42, 43). Later studies showed that this calcium transport across the mitochondrial inner membrane occurs through a uniporter, which transports calcium in an electrogenic manner, thereby dissipating the membrane potential generated by the respiratory chain, without requiring co-transport with an anion or exchange for another cation (44). Flux studies in isolated mitochondria suggested the existence of a channel mechanism that was remarkably selective for calcium (45). Subsequent studies showed that the primary route for mitochondrial calcium efflux is electroneutral exchange with sodium (46) or hydrogen (47, 48).

The molecular identity of the uniporter remained elusive until integrative genomic methods revealed its pore-forming protein MCU (49, 50), and regulatory subunits EMRE (51), MICU1 (52), MICU2 (53). Mitochondrial calcium uptake activity is abolished by mutations affecting key acidic residues in MCU act as a calcium selectivity filter (49).

The MCU homologue in dictyostelium discoideum is by itself sufficient to reconstitute mitochondrial calcium transport when expressed in yeast, which lacks uniporter components (54). However, human MCU alone is insufficient to transport calcium. EMRE, a metazoan specific protein that is part of the uniporter complex, is necessary for uniporter activity in mammalian cells. Heterologous co−expression of EMRE and human MCU is sufficient to reconstitute uniporter activity in yeast (51, 54). Furthermore, EMRE mediates the interaction of MCU with regulatory subunits MICU1 and MICU2 (51).

MICU1 and MICU2 function as a gatekeeper that sets the threshold of extra-mitochondrial calcium concentration for uptake of calcium into mitochondria (55-57). MICU2, which is a paralogue of MICU1, is closely linked to MICU1 both physically and functionally (53). Knockout of either MICU1 or MICU2 in mammalian cells results in mitochondria taking up calcium at a lower threshold of calcium concentration (56). The two components are localized to the inter-membrane space (52, 53). The emerging model is that the combination of MICU1 and MICU2 regulates the uniporter to prevent calcium at low concentration from passing through (58).

Genetic perturbation of uniporter components enables evaluation of how mitochondrial calcium uptake contributes to homeostasis and disease (59). On a cellular basis, perturbation of the uniporter is associated with apoptosis (60), the generation of mitochondrial reactive oxygen species (60), oncogene-induced senescence (61), matrix dehydrogenase activation and metabolic coupling (62), leukotriene receptor signaling (63), neuron excitotoxicity (64) and glucose stimulated insulin secretion (65). In whole animal models, loss of MCU can also be tolerated in mice with a mixed genetic background (62). These mice exhibit altered skeletal muscle metabolism and peak performance, however these mice did not have grossly altered cardiac function at baseline or in response to stress from an isoproterenol challenge or transverse aortic constriction.(62, 66) MCU knockout was found to be lethal for C57BL/6 mice, whereas knockout mice with an outbred CD1 background were viable (67). MCU knockout CD1 mice were overtly normal but had reduced exercise tolerance (67). Loss of uniporter activity in mice sinoatrial node cells through the overexpression of a dominant-negative

MCU protein revealed that mutant mice had a blunted increase in heart rate in response to β-adrenergic stimuli (68). Expressing this protein throughout the heart revealed altered cardiac oxygen utilization, cytoplasmic Ca^{2+} homeostasis, and pathologic responses to ischemia-reperfusion injury (69). MCU has also been shown to play a key role in matching cardiac metabolism to contractile stress (70, 71).

In humans, truncating mutations in MICU1 that lead to complete loss of its expression result in a Mendelian syndrome of skeletal muscle myopathy, learning disability and movement disorder (72). The impact of mutations in other uniporter components in human patients have not yet been reported.

Purpose of inquiry & Hypotheses

This thesis investigates the evolutionary history of the mitochondrial calcium uniporter and evaluates how mitochondrial uniporter dysfunction causes cardiac and vascular pathology.

The first part of this thesis systematically explores the taxonomic distribution and evolutionary history of the mitochondrial calcium uniporter. We hypothesize that systematic annotation of uniporter components across a range of diverse evolutionary taxa will enable inference about its evolutionary history. We test this hypothesis by utilizing the availability of a large and diverse array of recently sequenced eukaryotic genomes and systematically annotating these for the Uniporter. We then build a phylogenomic tree of eukaryotic life and analyze the gain and loss of uniporter components in the context of this phylogenomic tree.

The second part of this thesis describes the contribution of uniporter component MICU2 to cardiac and vascular homeostasis and pathophysiology. Transcriptome analysis of cardiomyopathy tissue from human patients and mouse models identifies >1000 genes that are differentially expressed in cardiomyopathy tissues (73, 74). We hypothesize that key mediators of cardiomyopathy should be consistently dysregulated in human patients with cardiomyopathy and mouse models of human cardiomyopathy. Hence these key mediators can be identified with a bioinformatic screen. Only six genes are consistently dysregulated across all transcriptome datasets, one of which is

uniporter component MICU2. We hypothesize that loss of MICU2 function will increase susceptibility to cardiovascular disease. We test this hypothesis profiling the cardiac and vascular phenotypes of a Micu2$^{-/-}$ knockout mouse.

Methods

Phylogenomic matrix of 162 eukaryotic species

Eukaryote genome and proteome data were downloaded from the KEGG Organisms Database, Release 58 (75). Six recently generated and annotated genomes were obtained from the Broad Institute Origins of Multicellularity Sequencing project (76): *T.trahens*, *C.owczarzaki*, *S.arctica*, *S.rosetta*, *A.macrogynus* and *S.punctatus*. Homologous proteins for each *M. musculus* protein were identified using pairwise BLASTP (77) (Expect<0.001) in each of the 162 sequenced eukaryotes, retaining the top homolog.

Phylogenomic tree reconstruction

A phylogenomic tree was constructed based on the methodology of Ciccarelli et al. (78). The following 16 highly conserved proteins (present in *E. coli* and in ≥98% of the 162 eukaryote genomes) were concatenated, interspersed with a 20-amino acid spacer sequences, and aligned using MUSCLE (79) (default parameters): Hars, Hspd1, Mlh1, Nthl1, Sars, Sod2, Top3a, Vars, Rps3, Uba2, Rpl23, Farsa, Ola1, Ddx47, Elp3, Qars. Five species were removed due to poor sequence alignment: *M.oryzae*, *M.guilliermondii*, *S.stipitis*, *P.placenta* and *X.laevis*. A species tree was constructed via Neighbor-Joining using MEGA 5.05 (80). Evolutionary distances were computed (Poisson correction) in units of amino acid substitutions per site assuming equal amino acid frequencies and substitution rates across sites, while correcting for multiple substitutions at a site. After removing ambiguous positions, there were 34844 pairwise aligned positions. Tree visualization was performed by iTOL (81), using the optimal tree with the sum of branch length of 26. The tree was manually compared to previous phylogenetic reconstructions (78, 82), and manually labeled with taxonomic branch names (e.g. Metazoa) for clarity. The reconstructed tree was consistent with published reconstructions (8, 19-24) or NCBI taxonomy except in four regions: mammals (Bos taurus, Canis lupus familiaris, Mus musculus, Sus scrofa), primitive metazoans (Nematostella vectensis, Hydra magnipapillata, Strongylocentrotus purpuratus, Trichoplax adhaerens), one insect (Pediculus humanus corporis), and three highly divergent fungal/protist species (Encephalitozoon cuniculi, Entamoeba histolytica,

Entamoeba dispar) perhaps due to well-established complications of phylogenomic reconstruction such as long-branch attraction (82).

Identification of MCU and MICU1 homologs

Putative homologs of *M. musculus* MCU and MICU1 were identified by bi-directional BLASTP homolog. These automated results required refinement, since for example the top BLASTP result for MCU in *B. Malayi* is Bm1_07575 which is not a bi-directional hit and lacks the DIME motif and protein structure fundamental to the uniporter. Therefore, putative MCU homologs were accepted as valid homolog if computational algorithms identified three features: (i) a conserved DIME motif when aligned with MUSCLE (79) or manual inspection, (ii) two transmembrane domains flanking the DIME motif as identified with TMHMM(83), (iii) two coiled-coil domains surrounding the transmembrane domains or circularly permuted as identified with COILS (84). One homolog lacking a coiled-coil domain was retained after inspection (Selaginella moellendorffii). Proteins were annotated for mitochondrial targeting sequences (MTS) with Mitoprot (85), but MTS presence was not required for homology.

We further explored the number of MCU homologs in each organism by counting how many proteins had a BLASTP top hit of MCU or CCDC109B and met this refinement criteria. Interestingly, three species of metaphyta (Vitis vinifera, Populus trichocarpa and Brachypodium distachyon) had MCU homologs containing chloroplast targeting signals in place of an MTS.

Bacterial homologs were identified by iterative PSI-BLASTP followed by manual inspection and by presence of DUF607 within the PFAM database. These two methods independently identified three putative homologs: Chlorobium phaeobacteroides A1BIL6, Prevotella oris D1QQZ1, and Cytophagia hutchinsonii Q11Z39. Each homolog contained conserved residues near the DIME motif (although the essential acidic residues were not conserved in C. phaeobacteroides), flanking transmembrane domains identified by TMHMM, and coiled-coil domains identified by COILS.

A similar refinement strategy was required for MICU1 homology, since in several species the EF-hand containing proteins *ARALAR1* and *SLC25A13* were identified as top BLASTP hits but are not bi-directional hits or functional homologs. Putative MICU1 homologs were considered valid if the alignment covered ≥80% of the query protein and

INTERPRO (86) identified ≥2 aligned EF-hand domains without additional protein domains (e.g. mitochondrial carrier protein domains).

MICU2 mouse generation

The *Micu2* mice were derived from the TG0122 (Efha1) gene-trap insertion site in the OST409343 OmniBank®ES cell line, which was acquired from Lexicon. The mice were backcrossed on to the C57/B6 background for >10 generations. All animal experiments and procedures were approved by the Harvard Medical School IACUC.

Mouse liver mitochondrial Isolation and calcium uptake analysis

Mitochondria were isolated from mouse liver using differential centrifugation as previously described (53) and resuspended in 220 mM mannitol, 75 mM sucrose, 10 mM HEPES pH 7.4, 1 mM EDTA, and 0.2% BSA and kept on ice. Calcium uptake assays were performed by adding 120 ug mitochondria to 150 uL buffer containing 125 mM KCl, 2 mM K_2HPO_4, 1 mM $MgCl_2$, 20 mM HEPES at pH 7.2, 5 mM glutamate and malate, and 1 μM Oregon Green-Bapta6F. Fluorescence was monitored using a Perkin-Elmer Envision plate reader in response to various pulses of $CaCl_2$. Relative rate of calcium uptake is reported using a linear fit of fluorescence from 30-40 s (n≥3).

Mouse echocardiography and abdominal ultrasonography

Mice were anesthetized with an isoflurane vaporizer (VetEquip), and each limb was placed on the ECG leads on a Vevo Mouse Handling Table (VisualSonics Inc.), maintaining the body temperature at 37°C during the study. Transthoracic echocardiography and trans-abdominal ultrasonography was performed using Vevo 2100 High-Resolution In Vivo Micro-Imaging System and MS550D transducer (VisualSonics Inc.), with heart rate at 500–550 bpm. The images were acquired as 2D (left parasternal long and short axes), M-mode (left parasternal short axis), speckle tracking and trans-abdominal 2D measurements. Measurements were averaged from images acquired during 3 consecutive heart beats. All echocardiographic and ultrasonographic measurements were performed with an experienced operator blinded to mouse genotype. Differences between groups of mice were determined using the unpaired Student's t-test.

Single Myocyte Functional Profiling

Ventricular cardiomyocytes from three pairs of adult WT and *Micu2*$^{-/-}$ littermates at 6-8 weeks of age on three separate days were isolated via a Langendorff-perfused heart preparation using enzymatic digestion as previously described.(87) After isolation, the cells were suspended in Tyrode's buffers with gradually increasing Ca^{2+} concentrations (0.06, 0.6, and 1.2 mM, pH 7.4 at room temperature) and were loaded with 1 μM fura-2AM calcium indicator (Molecular Probes, Eugene, OR, USA) as previously described.(88) Myocytes were washed 3 times for 10-15 minutes with 1.2 mM Ca^{2+} Tyrode's solution containing 250 μM probenecid to retain the indicator in the cytosol. The experiments were then performed at room temperature in 1.2 mM Ca^{2+} Tyrode's solution containing (in mM): NaCl 140, KCl 4.5, $MgCl_2$ 0.5, glucose 5, and HEPES 10, pH adjusted to 7.4 with NaOH.

Cardiomyocytes were electrically paced at 60 bpm via platinum wires. Sarcomere shortening/relengthening and fura-2 fluorescence ratios (which reflect the intracellular calcium transients) were simultaneously recorded and determined from discrete striation positions on the myocyte using a dual-excitation fluorescence imaging/contractility recording system (IonWizard® SarcLen detection and PMT Acquisition fluorescence system, IonOptix Inc., Milton, MA, USA). Sarcomere length and Ca^{2+} transients were analyzed using the IonOptix transient analysis software. Myocytes included in the study were rod-shaped with a clear striation pattern, quiescent in the absence of electrical stimulation and resting sarcomere length of more than 1.6 μm. A minimum of 7 myocytes were profiled from each animal. Statistical analysis was performed with a two sample one-tailed student t-test.

Electron microscopy

Left ventricular tissue from three pairs of wildtype and *Micu2*$^{-/-}$ littermates at 18 weeks of age were evaluated in a blinded fashion with 7 representative fields per mouse imaged at 1900x resolution on a Tecnai G² Spirit BioTWIN transmission electron microscope (FEI, Hillsboro, Oregon). The average mitochondrial size and eccentricity was automatically quantitated with CellProfiler (Broad Institute, Cambridge, MA).

Pharmacologic manipulation of blood pressure

To increase mouse blood pressure, mice were chronically infused with angiotensin II (Sigma-Aldrich) dissolved in saline at 1.4 mg/kg/day or 2.8 mg/kg/day or norepinephrine dissolved in saline at 5.6 mg/kg/day, via an osmotic minipump for two weeks. (89)

Blood pressure measurement

Systolic blood pressure was measured in trained conscious mice using a Visitech BP-2000 Analysis System (Visitech Systems, Apex, NC) as previously described.(90) Mice were restrained on a heated device to maintain body temperature during the measurements. The mice were "trained" to the procedure twice every day for 3 consecutive days, and data were recorded over the following 2 days. For each mouse, at least 10 readings were collected and used for statistical analysis.

Transcriptome wide analyses

Human tissue samples from HCM patients were obtained from study participants undergoing either myectomy heart surgery, cardiac transplant surgery, or valve replacement surgery under IRB approved protocols at Brigham and Women's Hospital.

RNA from human tissues and mouse LV was prepared and RNA-Seq libraries were constructed as previously described (91). Uniform amplification of the cDNA library was achieved with amplification cycling before the reaction reached saturation, as determined by quantitative PCR. Aorta RNA-Seq libraries were constructed with the Nextera library preparation method (92). To reduce biological variation in mouse specimens, RNA was pooled from three biological replicates for LV samples and Ang2 treated aorta samples. For the basal aorta RNA-Seq samples, libraries from three biological replicates for each genotype (Micu2$^{-/-}$ and wildtype) were constructed and the libraries were sequenced individually.

Libraries were sequenced on an Illumina HiSeq 2000 sequencer with 50 base pair paired-end reads. Following sequencing, alignment of reads to the mm10 genome was performed with Bowtie and Tophat (93). Gene expression profiles were constructed by tallying reads on gene loci, using a Bayesian P value to assess the significance of gene expression differences between pooled samples. (94) Cuffdiff 2 was used for

assessing significance of gene expression differences in aorta rna-seq library replicates.(95)

Genes were considered differentially expressed if there was a >40% increase or decrease in fold change with $p<10^{-3}$. The DCM mouse model and HCM mouse model transcriptome datasets were previously described. (74, 96) Gene ontology pathway enrichment analysis was performed with the Database for Annotation, Visualization, and Integrated Discovery (DAVID).(97)

Single Cell RNA-seq

Mouse aortas were dissected and digested into single cells using collagenase. Cells were captured, RNA extracted, and amplified into cDNA libraries using the Fluidigm C1 system (Fluidigm, San Francisco, CA) as previously described.(98) Libraries were sequenced on an Illumina HiSeq 2000 sequencer with 50 base pair paired-end reads. Reads were aligned using Tophat. The expression of known markers for vascular lineages was used to classify each cell as a smooth muscle cell (Acta2, Tagln, Myh11), fibroblast (Vim), or endothelial cell (Pecam1, Tek, Cdh5). Cells lacking any of these markers were classified as ‘undetermined.’ Wilcox and fisher test p-values were calculated in the R statistical computing environment, version 2.15.

Results

Evolutionary Diversity of the Mitochondrial Calcium Uniporter

We examined the phylogenomic distribution of the uniporter across 162 sequenced eukaryotic genomes, including six newly sequenced unicellular opisthokont/unikont genomes. First we constructed a eukaryotic tree of life based on 16 highly conserved proteins (Figure 1A and Figure 2). The tree is consistent with previous reconstructions of the eukaryotic tree of life and as expected places the newly sequenced unicellular opisthokonts between fungi and metazoans. Next we utilized a sequence similarity strategy followed by manual inspection to annotate organisms whose genomes harbor homologs of MCU and MICU1 (Figure 1A, B).

Homologs of MCU are widely distributed across major branches of eukaryotic life. They are present in all green plants and in virtually all metazoans, with the exceptions being the primitive metazoans *T. adherens* and *B. maylai* and the silkworm *B. mori*. As we previously reported, MCU homologs are missing in *S. cerevisiae*, and more generally, they are not found in any of the 22 non-filamentous fungi analyzed here. However, MCU homologs are found in a large number of filamentous fungi (e.g., *N. crassa*) as well as in many basidiomyces such as *C. neoformans* and *M. perniciosa*. As we previously reported, kinetoplastids harbor homologs of MCU (49, 50), but further analysis of protozoa indicate that they are absent in apicocomplexa, as well as in highly diverged mitosome-containing protozoa such as *G. lamblia* and *T. vaginalis*. The fact that MCU homologs are present in protists, fungi, metazoans, and plants suggest that it must have been an early feature of eukaryotic life and perhaps lost in certain fungal and protozoan lineages.

Genomes of most eukaryotes typically have both MCU and MICU1 homologs or lack both proteins (Figure 1A). Perhaps the most striking exception to this rule are MCU-containing fungi, where *MICU1* homologs have been lost altogether, suggesting that regulation of uniporter activity is fundamentally different in this clade. The earliest branching fungus, *A. macrogynus* is the sole exception, which contains both MCU and MICU1 homologs. Interestingly, greater diversity in MCU coiled-coil domain structure is also observed in these fungi. For example, *C. neoformans* and *M. perniciosa* show circularly permuted arrangements of coiled-coil domains rather than a coiled-coil

domains bracketing the transmembrane domain as is typically observed (Figure 1b). While the circularly permuted coiled-coil domain arrangement is not unique to the fungi (e.g. *A. thaliana*), the increased protein divergence may be coincident with the loss of MICU1. Only two organisms (*T. adherens*, *B*. *mori*) lacking MCU have homologs of MICU1*,* raising the hypothesis that mitochondria from these organisms either do not uptake calcium or have an alternate channel. As *MICU1* homologs are also found in protozoa, plants, metazoans, and unicellular opisthokonts, it is likely that the earliest eukaryote also harbored this regulator, but lost in fungal and certain protozoal lineages.

We previously reported that human MCU and MICU1 physically interact and are strongly co-expressed across different mammalian organs (49). One mechanism for ensuring co-expression in space and time is co-localization within the genome. Interestingly, while *MICU1* and *MCU* are not adjacent to each other in most of the analyzed genomes, all vertebrate genomes harbor these genes adjacent to each other, with a potential bi-directional promoter (Figure 1C), offering a mechanistic basis for their coordinate expression in vertebrates.

Finally we asked if any bacteria harbor homologs of this new class of calcium channels. Iterative sequence similarity and protein domain searches revealed in three diverse Bacteroidetes/Chlorobi group bacteria (*Prevotella oris*, *Chlorobium phaeobacteroides*, and *Cytophaga hutchinsonii*) putative MCU homologs that we now term “mitochondrial uniporter homologs” (*uni*). The *C. hutchinsonii uni* is particularly intriguing given its highly similar domain organization and conservation of residues essential for calcium transport (Figure 1B). Clearly, functional studies are required to determine if bacterial *uni* proteins are also cationic channels. If shown to transport calcium, they would represent the first prokaryotic calcium channels.

Integrative Transcriptomic Analysis implicates Mitochondrial Calcium Uniporter Regulatory Subunit MICU2 in Cardiovascular Homeostasis

Our bioinformatic screen intersected nine differentially expressed left ventricle transcriptome datasets. Seven datasets are derived from human heart tissue from patients with HCM (Table 1). Two datasets are derived from mouse models of DCM (PLN p.R9C)(99) and HCM (MYH6 p.R403Q)(100). Only six genes are consistently

differentially expressed across all nine transcriptome profiles: *MICU2, DAPK3, PRKAB2, IGFBP6, RHEB and UCP2* (Figure 3A).

MICU2, a calcium sensing regulatory subunit of the mitochondrial calcium uniporter complex localized in the mitochondrial intermembrane space (49, 53, 57), is a particularly intriguing candidate as cardiac calcium dysregulation is frequently observed in cardiomyopathy, and mitochondrial calcium overload is a key determinant in ischemic heart failure (101, 102). Furthermore recent studies link *Mcu*, the gene encoding the pore forming subunit of the mitochondrial calcium uniporter, to cardiac and skeletal muscle phenotypes. In particular, on a cellular level *Mcu* plays a key role in matching cardiac metabolism to contractile stress (70, 71) and controlling heart rate.(68) A $Mcu^{-/-}$ knockout mouse characterized by Finkel and colleagues, exhibits altered skeletal muscle metabolism and peak performance, however these mice did not have grossly altered cardiac function at baseline or in response to stress from an isoproterenol challenge or transverse aortic constriction (62, 66). Notably, a distinct dominant negative *Mcu* mouse model described by Anderson and colleagues had altered cardiac oxygen utilization, cytoplasmic Ca^{2+} homeostasis, and pathologic responses to ischemia-reperfusion injury.(69) Thus we prioritized *MICU2* for further characterization.

As altering cellular calcium prevents the development of cardiomyopathy in a mouse model (103), we hypothesize that increased *MICU2* expression may be a cardio-protective compensatory mechanism in the face of cardiac remodeling and thus deletion of *MICU2* would result in cardiac dysfunction.

Characterization of a global MICU2 knockout mouse

To evaluate the role of *MICU2* in cardiovascular homeostasis, we generated a global $Micu2^{-/-}$ mouse using a gene trap vector (Figure 3B, Figure 4A; see Methods). Mating $Micu^{+/-}$ x $Micu^{+/-}$ mice produced $Micu^{+/-}$, and $Micu2^{-/-}$ offspring in expected Mendelian ratios. $Micu^{+/-}$, and $Micu2^{-/-}$ mice were of identical size to wild-type littermates and routinely lived >18 months. As expected, the $Micu2^{+/-}$ mouse had approximately 50% Micu2 expression in hepatic, renal and cardiac tissue and the $Micu2^{-/-}$ mouse expressed 0.05-0.15 fold normal Micu2 mRNA levels in heart, kidney and liver (Figure 4B). Micu2 protein was significantly reduced on immunoblot of both $Micu2^{-/-}$ mouse left ventricle and liver tissue (Figure 3C, Figure 4C). Consistent with

prior results of RNAi targeting *Micu2* in mouse liver (53), Micu1 and Mcu protein levels were significantly reduced in the *Micu2*$^{-/-}$ mouse in liver tissue (Figure 4C). In the heart, Mcu protein expression was reduced by ~30% by immunoblot densitometry (Figure 3C). Also consistent with prior results, *Micu2*$^{-/-}$ mitochondria take up a high concentration pulse of calcium more slowly than wildtype mitochondria (56), but uptake a small pulse of calcium more rapidly (Figure 5), consistent with a role for MICU2 in setting the threshold for the uniporter. Together these results demonstrate that the *Micu2*$^{-/-}$ mouse is functionally deficient in *Micu2* protein activity.

We characterized the cardiac structure and function of *Micu2*$^{-/-}$ mice with histology, electron microscopy and longitudinal echocardiography. *Micu2*$^{-/-}$ mice and wildtype littermates had histologically indistinguishable hearts without evidence of differences in cellularity, cell size, or fibrosis (Figure 3, D and E). We observed no gross ultrastructural differences in sarcomere structure in *Micu2*$^{-/-}$ cardiac tissue by electron microscopy (Figure 3, F and G). However, mitochondria average area in *Micu2*$^{-/-}$ mice was ~20% smaller than wildtype mice ($p=0.003$; see Methods) and the *Micu2*$^{-/-}$ mice mitochondria tended to be ~5% more eccentric ($p=0.002$; see Methods; n: >1000 mitochondria measured from wild-type and mutant hearts) on automated quantification of mitochondria size and shape.

Micu2$^{-/-}$ mice have left atrial enlargement at 16-18 months of age on longitudinal echocardiography (20% increased diameter, $p=0.01$, Figure 3H, see Methods). No significant differences were identified in ventricular chamber dimensions or fractional shortening. (Figure 3I, Table 2). As left atrial enlargement reflects the cumulative effect of increased ventricular filling pressure over time, which exists in diastolic dysfunction, (104, 105), we hypothesized that these echocardiographic measurements were consistent with diastolic cardiac dysfunction.

To better characterize the cellular basis of *Micu2*$^{-/-}$ diastolic dysfunction, we performed single myocyte functional studies and global transcriptional studies of left ventricular myocardium (see Methods). We isolated myocytes from three pairs of WT and *Micu2*$^{-/-}$ littermates at 6-8 weeks of age and profiled the sarcomere contractility and cytosolic calcium transients.

Consistent with diastolic dysfunction, isolated single cardiomyocytes from *Micu2*$^{-/-}$ mice have altered relaxation kinetics (Figure 6, A and B, Table 3). In particular, *Micu2*$^{-/-}$ cardiomyocytes have similar contraction as *wildtype* cardiomyocytes as characterized by change in sarcomere length and speed of contraction, but *Micu2*$^{-/-}$ cardiomyocytes have a decreased rate of relaxation (p=0.02).

As myocyte contractility and relaxation kinetics are determined, at least in part, by cytosolic calcium fluxes, we hypothesized that *Micu2*$^{-/-}$ mice would have altered cytosolic calcium transients (Figure 6, A and B, Table 4). *Micu2*$^{-/-}$ cardiomyocytes have similar magnitude calcium fluxes as wildtype cardiomyocytes, however the time constant for calcium reuptake was increased in *Micu2*$^{-/-}$ cardiomyocytes (p=0.03). Together the cardiomyocyte profiling suggests that individual cardiomyocytes in *Micu2*$^{-/-}$ mice are slower to reuptake cytosolic calcium causing a decreased rate of myocyte relaxation. In aggregate, this cellular phenotype results in diastolic dysfunction.

Global transcriptional profiling with RNA-seq identified significant transcriptional differences in left ventricular tissue of Micu2$^{-/-}$ mice compared to wildtype littermates at 18 weeks of age. 781 genes were differentially expressed. We analyzed these genes in an unbiased way with DAVID gene set enrichment analysis, and observed significant enrichment in four gene ontologies (Figure 6C): sarcomere genes (Fold enrichment: 5.9, $p=6x10^{-8}$), bZIP transcription factors (Fold enrichment: 8.1, $p=1.1x10^{-8}$), stress response (Fold: 7.1, p=0.01), ribosomal proteins (Fold 8.4, p=0.002). We partitioned the differentially expressed gene list into genes that are primarily expressed (defined as >5 fold difference in expression between myocytes and fibroblasts) in myocytes (n=64) and primarily expressed in fibroblasts (n=89), with the remainder of the genes expressed in both fibroblasts and myocytes. Repeating the pathway analysis on these two gene sets, identified the sarcomere gene enrichment and oxidative phosphorylation in the myocyte subset and the bZIP transcription factor enrichment in the fibroblast gene subset. We further considered a manually curated gene set of 18 genes consistently observed as differentially regulated in left ventricular tissue in animals with cardiac hypertrophy (*Myh6, Myh7, Acta2, Fhl1, Fhl2, Nppa, Nppb, Col1a1, Postn, S100a4, Tgfb1, Tgfb2, Tgfb3, Clu, Xirp2, Tnni3, Tnnt2, Rcan1*). Seven of the eighteen (*Myh7, Acta2, Clu, Nppa, Nppb, Rcan1, Xirp2*) were differentially expressed (OR: 15, $p:4x10^{-6}$). We also

considered a previously described set of 1100 genes that encode for mitochondrial proteins (30, 106). Only 46 of the differentially expressed genes in the left ventricular tissue were included in this set (OR 1.1, p=NS), suggesting that the altered gene expression were not confined to the mitochondrial organelle. Two of the most significant changes in the RNA-seq dataset, were a 1.6 fold down regulation of sarcomere component *Myh7* (p<1e-50) and a 2.9 fold down regulation of the apelin receptor (*Aplnr; p=1e-40*) in *Micu2*$^{-/-}$ left ventricles. The magnitude of these changes were independently confirmed with qPCR of whole heart tissue (Figure 6D).

Angiotensin 2 induces cardiac and vascular dysfunction in Micu2$^{-/-}$ mouse

Next we evaluated whether Micu2$^{-/-}$ hearts display exacerbated pathologic phenotypes in response to pharmacologic stimuli of cardiac hypertrophy, angiotensin 2 (107). We hypothesized that *Micu2*$^{-/-}$ mice might be particularly sensitive to angiotensin 2, because the apelin receptor (*Aplnr)* suppresses angiotensin II type 1 receptor signaling via allosteric trans-inhibition (108, 109) and *Aplnr* was transcriptionally down regulated. Homozygous *Micu2*$^{-/-}$ mice, heterozygous *Micu2*$^{+/-}$ mice and wildtype littermates were infused with 1.2 mg/kg/day of angiotensin 2, which resulted in an equivalent ~25 mmHg increase in systolic blood pressure over baseline (p<0.001, Figure 7A). *A*fter 2 weeks of angiotensin 2 infusion, all three sets of mice had equivalent increases in cardiac wall thickness suggesting that all had the same degree of hypertrophic remodeling (Figure 7B). While the wildtype mice had no significant change in fractional shortening compared to baseline, *Micu2*$^{+/-}$ mice and *Micu2*$^{-/-}$ mice had a significant decrease in fractional shortening, a measure of systolic cardiac function (p=0.04 and p=0.002 respectively, Figure 7C). *Micu2*$^{-/-}$ mice also had significantly less fractional shortening than wildtype mice given the same dose of Ang2. Consistent with decreases in fractional shortening, Micu2$^{-/-}$ hearts also decreased systolic strain (p=0.007, Figure 7D) as measured by cardiac ultrasound speckle tracking imaging.

While evaluating the effect of angiotensin 2 induced hypertension on *Micu2*$^{-/-}$mice (1.2 mg/kg/day), three of fourteen *Micu2*$^{-/-}$ mice died unexpectedly within the first week from abdominal aortic aneurysm rupture as manifest by hemoperitoneum on postmortem exam (p=0.03, Figure 8A). This suggested *Micu2* plays a role in vascular homeostasis.

We tested the hypothesis that abdominal aorta dilatation of *Micu2*$^{-/-}$ was angiotensin 2 dose dependent. *Micu2*$^{-/-}$ mice were infused with either 1.2 mg/kg/day or 2.4 mg/kg/day of angiotensin 2 and blood pressure and aortic dimensions were measured. The higher angiotensin 2 dose elevated blood pressure significantly more than the lower dose (Figure 7A). Abdominal aortic diameter was measured with ultrasound after 2 weeks of angiotensin 2 treatment (Figure 8B). Absent angiotensin 2, *Micu2*$^{-/-}$ mice have approximately 5% larger abdominal aortic artery diameters on abdominal aorta ultrasound than wildtype mice (p=0.002). *Micu2*$^{-/-}$ mice had significantly larger abdominal aorta diameters and the angiotensin 2 effect was dose dependent (*Micu2*$^{-/-}$ genotype: p=0.0003, Ang2 dose: p=0.0006). Estimated conservatively, since those *Micu2*$^{-/-}$ mice with ruptured their aortas could not be assessed by ultrasound but likely had the largest aortic diameters, *Micu2*$^{-/-}$ aortas increased at least 4.5 fold more than wildtype aortas in response to angiotensin 2.

To evaluate when the abdominal aorta diameters in *Micu2*$^{-/-}$ mice increased compared to wildtype mice, we measured abdominal aorta diameters serially using ultrasound (Figure 8C, Table 5). Both *Micu2*$^{-/-}$ mice and wildtype mice abdominal aortas increased by ~10% on the second day. By day four, the diameter of the *Micu2*$^{-/-}$ mice had significantly (p=0.005) larger abdominal aortas. The *Micu2*$^{-/-}$ mice continued to increase in diameter, while the wildtype aorta diameter stabilized (Figure 8C).

To determine if the increased aortic diameter was specific to angiotensin 2 or reflected blood pressure elevation in general, hypertension was induced in Micu2-/- with norepinephrine. The norepinephrine dose (5.6 mg/kg/day) equivalently elevated blood pressure as 1.2 mg/kg/day angiotensin 2 dosing (Figure 7A). Notably, mice treated with norepinephrine had no increased abdominal aortic diameter over baseline, suggesting that abdominal aortic dilatation phenotype is specifically angiotensin 2 mediated and not solely due to elevated blood pressure (Figure 8B).

Global and Single-Cell Transcriptional profiling of Micu2$^{-/-}$ mouse aorta suggests mechanism for Angiotensin 2 induced aneurysm formation

We used RNA-seq and pathway analysis to compare mRNA levels in *Micu2*$^{-/-}$ and wild-type aortas. RNAseq analyses of three pairs of aortas from 8-12 week old *Micu2*$^{-/-}$ mice and wildtype littermates in the basal state and after two weeks of

angiotensin 2 infusion (1.2 mg/kg). In the basal state, 478 genes were significantly down-regulated and 819 genes were significantly up-regulated in *Micu2*$^{-/-}$ mice compared to wildtype. Pathway analysis in DAVID identified enrichment in 23 pathways from the set of down-regulated genes and 18 pathways from the set of up-regulated genes (Figure 9A). Notably up-regulated gene sets, significant after Bonferroni correction, include genes enriched in oxidation reduction reactions (3.7 fold enrichment, $p=6.2 \times 10^{-28}$), mitochondrial genes (2.8 fold enrichment, $p=2.4 \times 10^{-35}$) and genes related to the peroxisome (7.0 fold enrichment, $p=6.0 \times 10^{-13}$). Notably down-regulated gene sets include myofibril (9.2 fold enrichment, p=1.6 x 10-16), extracellular matrix (5.3 fold enrichment, $p=6.59 \times 10^{-10}$), cell adhesion (3.4 fold enrichment, $p=3.1 \times 10^{-12}$), blood vessel development (3.3 fold enrichment, p=0.01), growth factor binding (6.2 fold enrichment, p=0.002) and Wnt signaling (4.8 fold enrichment, p=0.002). These baseline differences in Micu2 deficient mice are consistent with a 5% increased abdominal aortic artery diameters (p=0.002, Figure 9B) in the absence of angiotensin 2 treatment and an increased susceptibility to angiotensin mediated aneurism development. Notably, while there is some overlap between the myofibril gene set and the sarcomere gene set dysregulated in the heart, the majority of these enrichment categories were not transcriptionally dysregulated in the heart, demonstrating tissue specificity of the Micu2$^{-/-}$ phenotype.

To identify how angiotensin 2 alters aorta transcriptional profiles, we performed pathway analysis on genes differentially expressed in the angiotensin 2 treated mice that were not differentially expressed in the basal state. This set included 180 up-regulated genes and 603 down-regulated genes, which fell in 7 up-regulated pathways and 9 down-regulated pathways. Transcription of inflammatory response genes (7 fold enrichment, $p=8.7 \times 10^{-5}$) and extracellular matrix genes (7.2 fold, 3.2×10^{-9}) were significantly enriched in the set of up-regulated genes and transcription of cell junction genes were enriched in the set of down-regulated genes (2.8 fold, $p=4.4 \times 10^{-4}$).

Abdominal aortic aneurysms may result from changes in the intima, media or adventitial layers, which are a heterogeneous collection of fibroblast, smooth muscle and endothelial cells. Histologic evaluation of *Micu2*$^{-/-}$ and wildtype mouse aortas did not favor one subset of cells (Figure 8A, inset). Because the aorta consists of primarily

smooth muscle cells and fibroblasts, we assessed which cell type was most perturbed by angiotensin 2 in wildtype and Micu2-/- aortas.

To deconvolute cellular transcriptional heterogeneity and characterize the early transcriptional changes present in *Micu2*$^{-/-}$ mouse aortas, we utilized single cell RNA-seq. Single cells from wildtype and *Micu2*$^{-/-}$ aortas after four days of angiotensin 2 treatment were captured on a microfluidic chip, reverse-transcribed to cDNA, barcoded and amplified. The resulting libraries were sequenced. About 60 smooth muscle and fibroblast cells were isolated from angiotensin 2 treated Micu2-/- and wildtype aortas (Figure 9D). Few endothelial cells were captured, likely due to their smaller cell diameter relative to the size of the microfluidic capture chip. The relative distribution of cell types was the same in the Micu2-/- and wildtype aortas (p=NS).

In the wildtype aorta, *Micu2* was robustly expressed in 50% of the endothelial cells, 23% of smooth muscle cells and 18% of fibroblast cells sequenced. This was further suggested by robust lacZ staining of all layers of the *Micu2*$^{-/-}$ abdominal aorta. Thus absence of *Micu2* may affect all of these cell types.

Two patterns of gene expression differences were observed: (1) differences in the absolute level of gene expression, quantitated with a Wilcox test on median difference (Figure 9E) and (2) differences in the number of cells that expressed a given gene at an appreciable level, quantitated with a Fisher test (Figure 9F). A bonferoni-adjustment for significance was set at $p<1x10^{-5}$ to reflect the ~5,000 genes expressed. At this strict threshold, six genes were differentially expressed in smooth muscle cells and five genes were differentially expressed in fibroblasts. Analysis of endothelial cells was underpowered as only 10 cells were captured, consequently, no genes exceeded the significance threshold.

Among the six genes differentially expressed in smooth muscle cells, notable differences include upregulation of genes associated with increased inflammatory and reactive oxygen species (ROS) states in *Micu2*$^{-/-}$ cells (Figure 9, E and F). Significantly more *Micu2*$^{-/-}$ smooth muscle cells expressed extracellular glutathione peroxidase *Gpx3* (96% of *Micu2*$^{-/-}$, 29% of wild type cells), inflammatory cytokines *Tnfaip6* and *Ccl11* as well as transcription factor *Irf1*, which is associated with inflammatory state. Also, while the majority of both *Micu2*$^{-/-}$ and wildtype smooth muscle cells expressed

metallothionein Mt1 which contributes to cardiovascular protection in high ROS states, the median expression was 9 fold higher in *Micu2*$^{-/-}$ smooth muscle cells ($p=7.5 \times 10^{-8}$).

The five genes differentially expressed in *Micu2*$^{-/-}$ fibroblasts are involved in proliferative response, inflammation and ROS (Figure 9, E and F). Of the *Micu2*$^{-/-}$ fibroblasts, 80% expressed the pro-proliferative transcription factor *Myc* compared to 10% of WT cells ($p=1.5 \times 10^{-6}$). Concordantly, *Nme2*, a negative regulator of Rho signaling, which activates *Myc*, had two-fold decreased expression in the *Micu2*$^{-/-}$ fibroblasts ($p=4.9 \times 10^{-6}$). 88% of *Micu2*$^{-/-}$ fibroblasts expressed *Efemp1,* which induces EGFR autophosphorylation and downstream activation of cell adhesion and migration, compared to 10% of the WT fibroblasts (9.6×10^{-8}). Concordantly, *Egr1*, an activator of differentiation and mitogenesis genes, had three-fold increased expression in *Micu2*$^{-/-}$ fibroblasts ($p=2.5 \times 10^{-6}$). *Micu2*$^{-/-}$ fibroblasts also had differential gene expression of inflammatory and ROS genes including significantly decreased expression of *Fmo3* and *Sod3* which reduce ROS free radicals and differential expression of inflammatory mediators *Il6* and *C1qb*.

Discussion, Conclusions, and Future Work

Evolutionary Diversity of the Mitochondrial Calcium Uniporter

Calcium uptake by mitochondria was discovered at the same time that mechanisms of chemiosmotic coupling were being deciphered, yet the molecular basis has only recently been resolved. The presence of MCU and MICU1 homologs in all major branches of eukaryotic life, suggest that it may play a far more fundamental role in eukaryotic cell physiology than previously anticipated. Our characterization of the uniporter's phylogenomic distribution and protein structures may guide physiological studies that may help establish the role of this channel in primitive eukaryotes, and may aid in elucidating its regulatory mechanisms. The putative identification of bacterial homologues of MCU, if experimentally confirmed, will be among the first calcium channels identified in bacteria.

Role of Micu2 in Cardiac Homeostasis

Our data establish a critical role for the mitochondrial calcium uniporter and specifically *Micu2* in maintaining both cardiac and vascular homeostasis in physiologic and pathophysiologic states. The absence of *Micu2* in normal physiologic states is associated with echocardiographic measurements consistent with cardiac diastolic dysfunction (isolated left atrial enlargement) and a decreased rate of relaxation on a single myocyte profiling. Myocytes lacking *Micu2*, have an increased time constant for cytosolic calcium reuptake suggesting a cellular mechanism. The physiologic stress of these altered calcium dynamics is evidenced by the transcriptional signature of *Micu2*$^{-/-}$ cardiac tissue which is characterized by sarcomere dysregulation, stress response pathways and altered expression of sarcomere genes and bZIP family of transcription factors, which are associated with cardiomyopathy pathogenesis (9, 10, 110-112).

In pathophysiologic cardiovascular states, the importance of *Micu2* is even more evident. In the setting of hypertension, *Micu2* knockout mice exhibit systolic cardiac dysfunction as evidenced by decreased fractional shortening and altered systolic strain measurements on speckle tracking imaging. Thus the hypertension stimuli appear to accelerate and accentuate the observed natural phenotype of left atrial enlargement with diastolic dysfunction. Although heart failure in the setting of normal cardiac dimensions termed "heart failure with preserved ejection fraction" is increasingly

observed clinically (113), animal models have yet to replicate this disease trajectory. The *Micu2*$^{-/-}$ mice, which have diastolic dysfunction but normal cardiac dimensions, may represent a first step in this direction.

Mechanistically, the molecular pathways underlying diastolic dysfunction are incompletely understood. On a cellular level, cardiomyocyte relaxation requires tightly bound actin-myosin filaments to detach, which is mediated by decreased levels of cytosolic calcium, hence any process that reduces calcium resequestration into cellular calcium stores (eg sarcoplasmic reticulum, mitochondria) or extrusion out of the cell can result in delayed relaxation (114). Proteins implicated in altered calcium handling in failing hearts include: the sarcoplasmic reticular Ca2+-ATPase (SERCA2a) and its modulator phospholamban (PLB); the SR–Ca2+ release channel and its modulator FK-506 binding protein 12.6 (FKBP12.6), and the sodium-calcium exchanger (NCX) (115-118). It is possible that MICU2 acts similarly to the PLB or FKBP12.6 proteins, sensing calcium levels outside mitochondria and dynamically gating the calcium uptake of the mitochondrial calcium uniporter.

Our data is consistent with other recent findings highlighting the importance of the mitochondrial calcium uniporter in maintaining cardiac homeostasis in physiologic and pathological states (62, 66, 68-71). However, diastolic cardiac dysfunction and systolic dysfunction in response to Angiotensin 2 has not previously been described. Whether the cardiac phenotype we observe in the *Micu2*$^{-/-}$ mice reflects differences in the molecular role of *Micu2* and *Mcu* or the specific nature of Angiotensin 2 perturbation or remains to be determined.

Overall, significant work remains to understand how the absence of *Micu2* gives rise to these physiologically significant changes to cardiac function. Mitochondrial calcium in general and the calcium uniporter is thought to be a relatively small calcium store in the context of the numerous ways that the cardiac myocyte buffers calcium (119). It is tempting to speculate that the loss of *Micu2* plays a role in altering the dynamics of calcium reuptake in the myocyte. In mitochondria from hepatocytes, which do not have significant other calcium buffering mechanisms, *Micu2*$^{-/-}$ mitochondria uptake high concentrations of calcium significantly more slowly than wildtype mitochondria (53, 56). However, the cardiac myocyte is flooded with high concentrations

of calcium with every contraction. Thus the slower mitochondrial calcium uptake may play a role in altering the cardiac calcium dynamics as evidenced by the decreased cytosolic calcium reuptake we observed.

Role of Micu2 in Vascular Homeostasis

In the setting of angiotensin 2 induced hypertension, *Micu2*$^{-/-}$ mice are prone to lethal abdominal aortic aneurysms. The transcriptional state of the *Micu2*$^{-/-}$ aorta is consistent with known transcriptional mechanisms of aneurysm formation involving a pro-inflammatory state with increased extracellular matrix remodeling and cellular proliferation in human patients and animal models (120-124). Matrix metalloproteinase 3 (Mmp3), which degrades collagen, fibronectin, laminin, and elastin is one of the most significantly upregulated genes. Polymorphisms in the *Mmp3* gene have been associated with aneurism formation in human patients(125, 126) and a mouse lacking *Mmp3* has reduced aneurism formation (127). Concordant with the collagen degradation induced by *Mmp3* upregulation, several collagens are unregulated after angiotensin 2 exposure including *Col3a1* and *Col1a2*, both of which are known causes of Ehlers-Danlos syndrome (128-130). Similarly other genes linked to familial aneurism syndromes, Fbn1 and Tgfb2 which are slightly downregulated in the basal state are upregulated after angiotensin 2 exposure (131-133).

Inflammatory response genes Serpina3n and Thbs1 are upregulated in response to Angiotensin 2. Serpina3n is an inhibitor of proapoptotic serine protease Granzyme B which contributes to aortic aneurysm through ECM cleavage. Serpina3n is a compensatory protective response to angiotensin 2 exposure.(134) Conversely, Thrombospondin-1 (Thbs1) contributes to a vascular pro-inflammatory state and aneurysm formation (135).

Insulin-like growth factor binding protein 2 (Igfbp2) was significantly down-regulated in the basal state and up-regulated after angiotensin 2 stimulation. Igfbp2 signals through epidermal growth factor receptor (EGFR) to potentiate STAT3 activation. Both Stat3 and Egfr are associated with abdominal aneurism formation in human patients and animal models (136, 137).

Calgranulins *S100a8* and *S100a4* are similarly downregulated in the basal state and upregulated after angiotensin infusion and may directly link altered calcium flux

caused by Micu2 to aneurysm. Calgranulins are a family of small acidic calcium signaling proteins that promote inflammation and vascular disease by activating RAGE(138) and are linked to vascular dysfunction and atherosclerosis.(139, 140) *S100a4* is strongly upregulated in the aortic wall of human thoracic aortic (141) and intracranial aneurysms (142). *S100a4* silencing decreases vascular smooth proliferation and matrix metalloproteinase expression (141).

Notably, the *Micu2*$^{-/-}$aneurysm phenotype is angiotensin 2 dose dependent but is not simply mediated by blood pressure as raising blood pressure with norepinephrine does not result in aortic dilatation, implicating Angiotensin 2 specific signaling. Angiotensin 2 has been shown to activate noncanonical TGFβ signaling (ERK1/2) via protein kinase C (143, 144). Altered TGF-Beta signaling is a common pathway of familial aortic aneurysm syndromes including FBN1 mutations associated with Marfan syndrome, TGFBR1/2 mutations associated with Loeys–Dietz and SMAD3/4 mutations associated with familial thoracic aortic aneurysms (131-133, 145). Recent work by Dietz and colleagues, demonstrated that mouse models of Marfan disease treated with calcium channel blockers, had accelerated thoracic aortic aneurysm expansion and rupture through a protein kinase C mediated pathway, suggesting that crosstalk between calcium signaling and TGFβ may cause aneurysms (146). Additionally, clinical evidence supports the link between calcium and aneurysm formation. For example, a large retrospective study of human patients with AAA found calcium channel blockers to be an independent risk factor for AAA (147). These results also motivate future investigation into how altered mitochondrial calcium homeostasis contributes to abdominal aortic aneurysms, as it is distinct from well described aneurysm syndromes

Angiotensin 2 is also known to mediate mitochondrial dysfunction via a protein kinase C dependent pathway by activating the endothelial cell NADPH oxidase and modulating $NO\cdot$ and O_2^- generation, which causes vascular dysfunction (148). Current rodent models of abdominal aortic aneurysms rely heavily on mice with atherogenic mutations and aneurysms in these mice are thought to be mediated by reactive oxygen species (149, 150). Loss of the *Micu2* paralog, *Micu1*, results in oxidative stress and vascular dysfunction (151). Thus given the transcriptional changes we observed in both whole tissue and single cell RNA-seq which reflect transcriptional changes associated

oxidative stress, it is likely that the *Micu2* mouse aneurysm is also caused by oxidative stress. Regardless, the *Micu2*$^{-/-}$ mouse described here represents a distinctly different mouse model from atherogenic mutation models and may provide new insights into disease pathogenesis and therapeutics. Future work in understanding the interplay between mitochondrial calcium homeostasis and AAA may identify new mechanisms amenable to therapeutic intervention.

Human patients with two *MICU2* loss of function mutations have not yet been reported. However, patients with *MICU1* homozygous loss of function mutations have a skeletal muscle myopathy and learning difficulties with extrapyramidal symptoms.(72) Although cardiovascular disease was not described as a phenotypic disease feature, *MICU1* and *MICU2* form a protein-protein complex (56), so it is possible that these patients have a subclinical cardiovascular phenotype or may develop cardiovascular disease in the future. Patients identified with *MICU2* loss of function mutations in the future should be closely followed for evidence of cardiovascular disease and may benefit from treatment that decreases angiotensin 2 signaling.

Summary

In this dissertation, I characterize the evolutionary origin of an ancient and ubiquitous biochemical process – the uptake of calcium by mitochondria and demonstrate that this function prevents cardiac and vascular disease. Calcium uptake into the mitochondria occurs via a recently identified macromolecular complex: the mitochondrial calcium uniporter. I first characterize the phylogenomic distribution of the uniporter's membrane spanning pore protein (MCU) and regulatory subunits (MICU1 and MICU2) across 162 eukaryotic genomes. Reconstructing a phylogenomic tree of life, reveals homologs of both MCU and MICU1 tend to co-occur in all major branches of eukaryotic life but both have been lost along certain protozoan and fungal lineages. Together this suggests that the uniporter was an early feature of mitochondria and that both pore and regulatory subunits are important in its function. The wide distribution of the uniporter, suggests that it plays an important role in eukaryotes.

Transcriptome wide analysis of human and mouse cardiomyopathy datasets identifies *MICU2* as consistently upregulated in disease. To test the hypothesis that increased *MICU2* expression is cardio-protective, we generated a global *Micu2*$^{-/-}$ mouse. At baseline, *Micu2*$^{-/-}$ mice have diastolic cardiac dysfunction. When stressed with angiotensin 2, *Micu2*$^{-/-}$ mice exhibit systolic cardiac dysfunction and developed lethal abdominal aortic aneurysms. Single-cell RNA-sequencing of the aorta identified differential reactive oxygen species, inflammation and proliferation in *Micu2*$^{-/-}$ aortas suggesting a mechanism for aneurism formation. Together, these data point to a significant and previously unappreciated role for *Micu2* in maintaining both cardiac and vascular homeostasis.

References

1. Heidenreich PA, Trogdon JG, Khavjou OA, Butler J, Dracup K, Ezekowitz MD, et al. Forecasting the Future of Cardiovascular Disease in the United States. Circulation. 2011;123(8):933-44. doi: 10.1161/CIR.0b013e31820a55f5.

2. Yancy CW, Jessup M, Bozkurt B, Butler J, Casey DE, Drazner MH, et al. 2013 ACCF/AHA Guideline for the Management of Heart Failure: A Report of the American College of Cardiology Foundation/American Heart Association Task Force on Practice Guidelines. Circulation. 2013;128(16):e240-e327. doi: 10.1161/CIR.0b013e31829e8776.

3. Djousse L, Driver JA, Gaziano JM. Relation between modifiable lifestyle factors and lifetime risk of heart failure. JAMA : the journal of the American Medical Association. 2009;302(4):394-400. Epub 2009/07/23. doi: 10.1001/jama.2009.1062. PubMed PMID: 19622818; PubMed Central PMCID: PMCPmc2742484.

4. Curtis LH, Whellan DJ, Hammill BG, et al. INcidence and prevalence of heart failure in elderly persons, 1994-2003. Archives of Internal Medicine. 2008;168(4):418-24. doi: 10.1001/archinternmed.2007.80.

5. Mozaffarian D, Benjamin EJ, Go AS, Arnett DK, Blaha MJ, Cushman M, et al. Heart disease and stroke statistics--2015 update: a report from the American Heart Association. Circulation. 2015;131(4):e29-322. doi: 10.1161/CIR.0000000000000152. PubMed PMID: 25520374.

6. Maron BJ. Hypertrophic cardiomyopathy: a systematic review. JAMA : the journal of the American Medical Association. 2002;287(10):1308-20. Epub 2002/03/12. PubMed PMID: 11886323.

7. Manolio TA, Baughman KL, Rodeheffer R, Pearson TA, Bristow JD, Michels VV, et al. Prevalence and etiology of idiopathic dilated cardiomyopathy (summary of a National Heart, Lung, and Blood Institute workshop. The American journal of cardiology. 1992;69(17):1458-66. Epub 1992/06/01. PubMed PMID: 1590237.

8. Mestroni L, Rocco C, Gregori D, Sinagra G, Di Lenarda A, Miocic S, et al. Familial dilated cardiomyopathy: evidence for genetic and phenotypic heterogeneity. Heart Muscle Disease Study Group. Journal of the American College of Cardiology. 1999;34(1):181-90. Epub 1999/07/10. PubMed PMID: 10400009.

9. Konno T, Chang S, Seidman JG, Seidman CE. Genetics of hypertrophic cardiomyopathy. Current opinion in cardiology. 2010. Epub 2010/02/04. doi: 10.1097/HCO.0b013e3283375698. PubMed PMID: 20124998; PubMed Central PMCID: PMC2932754.
10. Teekakirikul P, Padera RF, Seidman JG, Seidman CE. Hypertrophic cardiomyopathy: Translating cellular cross talk into therapeutics. The Journal of Cell Biology. 2012;199(3):417-21. doi: 10.1083/jcb.201207033.
11. Sulakhe PV, Dhalla NS. Excitation-contraction coupling in heart: VII. Calcium accumulation in subcellular particles in congestive heart failure. Journal of Clinical Investigation. 1971;50(5):1019-27. PubMed PMID: PMC292024.
12. Ingwall JS. Transgenesis and cardiac energetics: new insights into cardiac metabolism. Journal of Molecular and Cellular Cardiology. 2004;37(3):613-23. doi: http://dx.doi.org/10.1016/j.yjmcc.2004.05.020.
13. Maack C, O'Rourke B. Excitation-contraction coupling and mitochondrial energetics. Basic Res Cardiol. 2007;102(5):369-92. doi: 10.1007/s00395-007-0666-z.
14. Gao WD, Pérez NG, Seidman CE, Seidman JG, Marbán E. Altered cardiac excitation–contraction coupling in mutant mice with familial hypertrophic cardiomyopathy. Journal of Clinical Investigation. 1999;103(5):661-6. PubMed PMID: PMC408123.
15. Hasenfuss G, Mulieri LA, Leavitt BJ, Allen PD, Haeberle JR, Alpert NR. Alteration of contractile function and excitation-contraction coupling in dilated cardiomyopathy. Circulation Research. 1992;70(6):1225-32. doi: 10.1161/01.res.70.6.1225.
16. Palmer BM, Schmitt JP, Seidman CE, Seidman JG, Wang Y, Bell SP, et al. Elevated rates of force development and MgATP binding in F764L and S532P myosin mutations causing dilated cardiomyopathy. J Mol Cell Cardiol. 2013;57:23-31. Epub 2013/01/15. doi: 10.1016/j.yjmcc.2012.12.022. PubMed PMID: 23313350; PubMed Central PMCID: PMCPmc3594396.
17. Palmer BM, Fishbaugher DE, Schmitt JP, Wang Y, Alpert NR, Seidman CE, et al. Differential cross-bridge kinetics of FHC myosin mutations R403Q and R453C in heterozygous mouse myocardium. American journal of physiology Heart and circulatory

physiology. 2004;287(1):H91-9. Epub 2004/03/06. doi: 10.1152/ajpheart.01015.2003. PubMed PMID: 15001446.

18. Taegtmeyer H, King LM, Jones BE. Energy substrate metabolism, myocardial ischemia, and targets for pharmacotherapy. The American journal of cardiology. 1998;82(5, Supplement 1):54K-60K. doi: http://dx.doi.org/10.1016/S0002-9149(98)00538-4.

19. Territo PR, Mootha VK, French SA, Balaban RS. Ca2+ activation of heart mitochondrial oxidative phosphorylation: role of the F0/F1-ATPase2000 2000-02-01 00:00:00. C423-C35 p.

20. Depre C, Davies PJA, Taegtmeyer H. Transcriptional adaptation of the heart to mechanical unloading. The American journal of cardiology. 1999;83(12, Supplement 1):58-63. doi: http://dx.doi.org/10.1016/S0002-9149(99)00260-X.

21. Teekakirikul P, Eminaga S, Toka O, Alcalai R, Wang L, Wakimoto H, et al. Cardiac fibrosis in mice with hypertrophic cardiomyopathy is mediated by non-myocyte proliferation and requires Tgf-β. The Journal of Clinical Investigation. 2010;120(10):3520-9. doi: 10.1172/JCI42028.

22. Koopman WJH, Willems PHGM, Smeitink JAM. Monogenic Mitochondrial Disorders. New England Journal of Medicine. 2012;366(12):1132-41. doi: 10.1056/NEJMra1012478.

23. Lieber DS, Calvo SE, Shanahan K, Slate NG, Liu S, Hershman SG, et al. Targeted exome sequencing of suspected mitochondrial disorders. Neurology. 2013;80(19):1762-70. doi: 10.1212/WNL.0b013e3182918c40. PubMed PMID: PMC3719425.

24. Calvo S, Jain M, Xie X, Sheth SA, Chang B, Goldberger OA, et al. Systematic identification of human mitochondrial disease genes through integrative genomics. Nature genetics. 2006;38(5):576-82. Epub 2006/04/04. doi: 10.1038/ng1776. PubMed PMID: 16582907.

25. Calvo SE, Compton AG, Hershman SG, Lim SC, Lieber DS, Tucker EJ, et al. Molecular diagnosis of infantile mitochondrial disease with targeted next-generation sequencing. Science translational medicine. 2012;4(118):118ra10-ra10.

26. Götz A, Tyynismaa H, Euro L, Ellonen P, Hyötyläinen T, Ojala T, et al. Exome sequencing identifies mitochondrial alanyl-tRNA synthetase mutations in infantile mitochondrial cardiomyopathy. The American Journal of Human Genetics. 2011;88(5):635-42.
27. Brunetti-Pierri N, Pignatelli R, Fouladi N, Towbin JA, Belmont JW, Craigen WJ, et al. Dilation of the aortic root in mitochondrial disease patients. Molecular Genetics and Metabolism. 2011;103(2):167-70. doi: http://dx.doi.org/10.1016/j.ymgme.2011.02.007.
28. Tay SH, Nordli DR, Jr., Bonilla E, Null E, Monaco S, Hirano M, et al. Aortic rupture in mitochondrial encephalopathy, lactic acidosis, and stroke-like episodes. Archives of neurology. 2006;63(2):281-3. Epub 2006/02/16. doi: 10.1001/archneur.63.2.281. PubMed PMID: 16476819.
29. Vafai SB, Mootha VK. Mitochondrial disorders as windows into an ancient organelle. Nature. 2012;491(7424):374-83. doi: 10.1038/nature11707. PubMed PMID: 23151580.
30. Pagliarini DJ, Calvo SE, Chang B, Sheth SA, Vafai SB, Ong SE, et al. A mitochondrial protein compendium elucidates complex I disease biology. Cell. 2008;134(1):112-23. doi: 10.1016/j.cell.2008.06.016. PubMed PMID: 18614015; PubMed Central PMCID: PMC2778844.
31. Baynes J. Medical biochemistry. Fourth edition. ed. Dominiczak MH, editor: Saunders; 2014.
32. Gameiro PA, Laviolette LA, Kelleher JK, Iliopoulos O, Stephanopoulos G. Cofactor balance by nicotinamide nucleotide transhydrogenase (NNT) coordinates reductive carboxylation and glucose catabolism in the tricarboxylic acid (TCA) cycle. Journal of Biological Chemistry. 2013;288(18):12967-77.
33. Kaukonen J, Juselius JK, Tiranti V, Kyttälä A, Zeviani M, Comi GP, et al. Role of adenine nucleotide translocator 1 in mtDNA maintenance. Science. 2000;289(5480):782-5.
34. Pfanner N, Geissler A. Versatility of the mitochondrial protein import machinery. Nature Reviews Molecular Cell Biology. 2001;2(5):339-49.

35. Varanyuwatana P, Halestrap AP. The roles of phosphate and the phosphate carrier in the mitochondrial permeability transition pore. Mitochondrion. 2012;12(1):120-5.
36. Stefani DD, Rizzuto R, Pozzan T. Enjoy the Trip: Calcium in Mitochondria Back and Forth. Annual Review of Biochemistry. 2016;85(1):null. doi: doi:10.1146/annurev-biochem-060614-034216.
37. Cogswell AM, Stevens RJ, Hood DA. Properties of skeletal muscle mitochondria isolated from subsarcolemmal and intermyofibrillar regions. The American journal of physiology. 1993;264(2 Pt 1):C383-9. Epub 1993/02/01. PubMed PMID: 8383431.
38. Romashko DN, Marban E, O'Rourke B. Subcellular metabolic transients and mitochondrial redox waves in heart cells. Proceedings of the National Academy of Sciences. 1998;95(4):1618-23.
39. Saks VA, Kuznetsov AV, Vendelin M, Guerrero K, Kay L, Seppet EK. Functional coupling as a basic mechanism of feedback regulation of cardiac energy metabolism. Molecular and cellular biochemistry. 2004;256-257(1-2):185-99. PubMed PMID: 14977180.
40. Cortassa S, Aon MA, Marbán E, Winslow RL, O'Rourke B. An Integrated Model of Cardiac Mitochondrial Energy Metabolism and Calcium Dynamics. Biophysical Journal. 2003;84(4):2734-55. doi: http://dx.doi.org/10.1016/S0006-3495(03)75079-6.
41. Beutner G, Sharma VK, Lin L, Ryu S-Y, Dirksen RT, Sheu S-S. Type 1 ryanodine receptor in cardiac mitochondria: Transducer of excitation–metabolism coupling. Biochimica et Biophysica Acta (BBA) - Biomembranes. 2005;1717(1):1-10. doi: http://dx.doi.org/10.1016/j.bbamem.2005.09.016.
42. Deluca HF, Engstrom GW. Calcium uptake by rat kidney mitochondria. Proc Natl Acad Sci U S A. 1961;47:1744-50. PubMed PMID: 13885269; PubMed Central PMCID: PMC223205.
43. Vasington FD, Murphy JV. Ca ion uptake by rat kidney mitochondria and its dependence on respiration and phosphorylation. The Journal of biological chemistry. 1962;237:2670-7. PubMed PMID: 13925019.

44. Gunter TE, Pfeiffer DR. Mechanisms by which mitochondria transport calcium. The American journal of physiology. 1990;258(5 Pt 1):C755-86. PubMed PMID: 2185657.
45. Kirichok Y, Krapivinsky G, Clapham DE. The mitochondrial calcium uniporter is a highly selective ion channel. Nature. 2004;427(6972):360-4. doi: 10.1038/nature02246. PubMed PMID: 14737170.
46. Palty R, Silverman WF, Hershfinkel M, Caporale T, Sensi SL, Parnis J, et al. NCLX is an essential component of mitochondrial Na+/Ca2+ exchange. Proc Natl Acad Sci U S A. 2010;107(1):436-41. doi: 10.1073/pnas.0908099107. PubMed PMID: 20018762; PubMed Central PMCID: PMC2806722.
47. Tsai MF, Jiang D, Zhao L, Clapham D, Miller C. Functional reconstitution of the mitochondrial Ca2+/H+ antiporter Letm1. The Journal of general physiology. 2014;143(1):67-73. doi: 10.1085/jgp.201311096. PubMed PMID: 24344246; PubMed Central PMCID: PMC3874562.
48. Jiang D, Zhao L, Clapham DE. Genome-wide RNAi screen identifies Letm1 as a mitochondrial Ca2+/H+ antiporter. Science. 2009;326(5949):144-7. doi: 10.1126/science.1175145. PubMed PMID: 19797662; PubMed Central PMCID: PMC4067766.
49. Baughman JM, Perocchi F, Girgis HS, Plovanich M, Belcher-Timme CA, Sancak Y, et al. Integrative genomics identifies MCU as an essential component of the mitochondrial calcium uniporter. Nature. 2011;476(7360):341-5. doi: 10.1038/nature10234. PubMed PMID: 21685886; PubMed Central PMCID: PMC3486726.
50. De Stefani D, Raffaello A, Teardo E, Szabo I, Rizzuto R. A forty-kilodalton protein of the inner membrane is the mitochondrial calcium uniporter. Nature. 2011;476(7360):336-40. doi: 10.1038/nature10230. PubMed PMID: 21685888; PubMed Central PMCID: PMC4141877.
51. Sancak Y, Markhard AL, Kitami T, Kovacs-Bogdan E, Kamer KJ, Udeshi ND, et al. EMRE is an essential component of the mitochondrial calcium uniporter complex. Science. 2013;342(6164):1379-82. doi: 10.1126/science.1242993. PubMed PMID: 24231807; PubMed Central PMCID: PMC4091629.

52. Perocchi F, Gohil VM, Girgis HS, Bao XR, McCombs JE, Palmer AE, et al. MICU1 encodes a mitochondrial EF hand protein required for Ca(2+) uptake. Nature. 2010;467(7313):291-6. doi: 10.1038/nature09358. PubMed PMID: 20693986; PubMed Central PMCID: PMC2977980.
53. Plovanich M, Bogorad RL, Sancak Y, Kamer KJ, Strittmatter L, Li AA, et al. MICU2, a paralog of MICU1, resides within the mitochondrial uniporter complex to regulate calcium handling. PloS one. 2013;8(2):e55785. doi: 10.1371/journal.pone.0055785. PubMed PMID: 23409044; PubMed Central PMCID: PMC3567112.
54. Kovacs-Bogdan E, Sancak Y, Kamer KJ, Plovanich M, Jambhekar A, Huber RJ, et al. Reconstitution of the mitochondrial calcium uniporter in yeast. Proc Natl Acad Sci U S A. 2014;111(24):8985-90. doi: 10.1073/pnas.1400514111. PubMed PMID: 24889638; PubMed Central PMCID: PMC4066498.
55. Csordas G, Golenar T, Seifert EL, Kamer KJ, Sancak Y, Perocchi F, et al. MICU1 controls both the threshold and cooperative activation of the mitochondrial Ca(2)(+) uniporter. Cell Metab. 2013;17(6):976-87. doi: 10.1016/j.cmet.2013.04.020. PubMed PMID: 23747253; PubMed Central PMCID: PMC3722067.
56. Kamer KJ, Mootha VK. MICU1 and MICU2 play nonredundant roles in the regulation of the mitochondrial calcium uniporter. EMBO reports. 2014;15(3):299-307. doi: 10.1002/embr.201337946. PubMed PMID: 24503055; PubMed Central PMCID: PMC3989696.
57. Kamer KJ, Sancak Y, Mootha VK. The uniporter: from newly identified parts to function. Biochemical and biophysical research communications. 2014;449(4):370-2. doi: 10.1016/j.bbrc.2014.04.143. PubMed PMID: 24814702.
58. Patron M, Checchetto V, Raffaello A, Teardo E, Vecellio Reane D, Mantoan M, et al. MICU1 and MICU2 finely tune the mitochondrial Ca2+ uniporter by exerting opposite effects on MCU activity. Molecular cell. 2014;53(5):726-37. doi: 10.1016/j.molcel.2014.01.013. PubMed PMID: 24560927; PubMed Central PMCID: PMC3988891.

59. Kamer KJ, Mootha VK. The molecular era of the mitochondrial calcium uniporter. Nature reviews Molecular cell biology. 2015;16(9):545-53. doi: 10.1038/nrm4039. PubMed PMID: 26285678.
60. Mallilankaraman K, Doonan P, Cardenas C, Chandramoorthy HC, Muller M, Miller R, et al. MICU1 is an essential gatekeeper for MCU-mediated mitochondrial Ca(2+) uptake that regulates cell survival. Cell. 2012;151(3):630-44. doi: 10.1016/j.cell.2012.10.011. PubMed PMID: 23101630; PubMed Central PMCID: PMC3486697.
61. Wiel C, Lallet-Daher H, Gitenay D, Gras B, Le Calve B, Augert A, et al. Endoplasmic reticulum calcium release through ITPR2 channels leads to mitochondrial calcium accumulation and senescence. Nat Commun. 2014;5:3792. doi: 10.1038/ncomms4792. PubMed PMID: 24797322.
62. Pan X, Liu J, Nguyen T, Liu C, Sun J, Teng Y, et al. The physiological role of mitochondrial calcium revealed by mice lacking the mitochondrial calcium uniporter. Nature cell biology. 2013;15(12):1464-72. doi: 10.1038/ncb2868. PubMed PMID: 24212091; PubMed Central PMCID: PMC3852190.
63. Samanta K, Douglas S, Parekh AB. Mitochondrial calcium uniporter MCU supports cytoplasmic Ca2+ oscillations, store-operated Ca2+ entry and Ca2+-dependent gene expression in response to receptor stimulation. PloS one. 2014;9(7):e101188. doi: 10.1371/journal.pone.0101188. PubMed PMID: 25004162; PubMed Central PMCID: PMC4086884.
64. Qiu J, Tan YW, Hagenston AM, Martel MA, Kneisel N, Skehel PA, et al. Mitochondrial calcium uniporter Mcu controls excitotoxicity and is transcriptionally repressed by neuroprotective nuclear calcium signals. Nat Commun. 2013;4:2034. doi: 10.1038/ncomms3034. PubMed PMID: 23774321; PubMed Central PMCID: PMC3709514.
65. Alam MR, Groschner LN, Parichatikanond W, Kuo L, Bondarenko AI, Rost R, et al. Mitochondrial Ca2+ uptake 1 (MICU1) and mitochondrial ca2+ uniporter (MCU) contribute to metabolism-secretion coupling in clonal pancreatic beta-cells. The Journal of biological chemistry. 2012;287(41):34445-54. doi: 10.1074/jbc.M112.392084. PubMed PMID: 22904319; PubMed Central PMCID: PMC3464549.

66. Holmström KM, Pan X, Liu JC, Menazza S, Liu J, Nguyen TT, et al. Assessment of cardiac function in mice lacking the mitochondrial calcium uniporter. Journal of Molecular and Cellular Cardiology. 2015;85:178-82. doi: http://dx.doi.org/10.1016/j.yjmcc.2015.05.022.
67. Murphy E, Pan X, Nguyen T, Liu J, Holmstrom KM, Finkel T. Unresolved questions from the analysis of mice lacking MCU expression. Biochemical and biophysical research communications. 2014;449(4):384-5. doi: 10.1016/j.bbrc.2014.04.144. PubMed PMID: 24792186; PubMed Central PMCID: PMC4214067.
68. Wu Y, Rasmussen TP, Koval OM, Joiner M-lA, Hall DD, Chen B, et al. The mitochondrial uniporter controls fight or flight heart rate increases. Nat Commun. 2015;6. doi: 10.1038/ncomms7081.
69. Rasmussen TP, Wu Y, Joiner M-lA, Koval OM, Wilson NR, Luczak ED, et al. Inhibition of MCU forces extramitochondrial adaptations governing physiological and pathological stress responses in heart. Proceedings of the National Academy of Sciences. 2015;112(29):9129-34. doi: 10.1073/pnas.1504705112.
70. Kwong Jennifer Q, Lu X, Correll Robert N, Schwanekamp Jennifer A, Vagnozzi Ronald J, Sargent Michelle A, et al. The Mitochondrial Calcium Uniporter Selectively Matches Metabolic Output to Acute Contractile Stress in the Heart. Cell Reports. 2015;12(1):15-22. doi: http://dx.doi.org/10.1016/j.celrep.2015.06.002.
71. Luongo Timothy S, Lambert Jonathan P, Yuan A, Zhang X, Gross P, Song J, et al. The Mitochondrial Calcium Uniporter Matches Energetic Supply with Cardiac Workload during Stress and Modulates Permeability Transition. Cell Reports. 2015;12(1):23-34. doi: http://dx.doi.org/10.1016/j.celrep.2015.06.017.
72. Logan CV, Szabadkai G, Sharpe JA, Parry DA, Torelli S, Childs A-M, et al. Loss-of-function mutations in MICU1 cause a brain and muscle disorder linked to primary alterations in mitochondrial calcium signaling. Nature genetics. 2014;46(2):188-93. doi: 10.1038/ng.2851

http://www.nature.com/ng/journal/v46/n2/abs/ng.2851.html#supplementary-information.
73. Kim JB, Porreca GJ, Song L, Greenway SC, Gorham JM, Church GM, et al. Polony multiplex analysis of gene expression (PMAGE) in mouse hypertrophic

cardiomyopathy. Science. 2007;316(5830):1481-4. doi: 10.1126/science.1137325. PubMed PMID: 17556586.
74. Christodoulou DC, Wakimoto H, Onoue K, Eminaga S, Gorham JM, DePalma SR, et al. 5′RNA-Seq identifies Fhl1 as a genetic modifier in cardiomyopathy. The Journal of Clinical Investigation. 2014;124(3):1364-70. doi: 10.1172/JCI70108. PubMed PMID: PMC3934171.
75. Kanehisa M, Goto S, Hattori M, Aoki-Kinoshita KF, Itoh M, Kawashima S, et al. From genomics to chemical genomics: new developments in KEGG. Nucleic acids research. 2006;34(Database issue):D354-7. Epub 2005/12/31. doi: 10.1093/nar/gkj102. PubMed PMID: 16381885; PubMed Central PMCID: PMC1347464.
76. Ruiz-Trillo I, Burger G, Holland PW, King N, Lang BF, Roger AJ, et al. The origins of multicellularity: a multi-taxon genome initiative. Trends in genetics : TIG. 2007;23(3):113-8. Epub 2007/02/06. doi: 10.1016/j.tig.2007.01.005. PubMed PMID: 17275133.
77. Altschul SF, Madden TL, Schaffer AA, Zhang J, Zhang Z, Miller W, et al. Gapped BLAST and PSI-BLAST: a new generation of protein database search programs. Nucleic acids research. 1997;25(17):3389-402. Epub 1997/09/01. PubMed PMID: 9254694; PubMed Central PMCID: PMC146917.
78. Ciccarelli FD, Doerks T, von Mering C, Creevey CJ, Snel B, Bork P. Toward automatic reconstruction of a highly resolved tree of life. Science. 2006;311(5765):1283-7. Epub 2006/03/04. doi: 10.1126/science.1123061. PubMed PMID: 16513982.
79. Edgar RC. MUSCLE: multiple sequence alignment with high accuracy and high throughput. Nucleic acids research. 2004;32(5):1792-7. Epub 2004/03/23. doi: 10.1093/nar/gkh340. PubMed PMID: 15034147; PubMed Central PMCID: PMC390337.
80. Tamura K, Peterson D, Peterson N, Stecher G, Nei M, Kumar S. MEGA5: Molecular Evolutionary Genetics Analysis Using Maximum Likelihood, Evolutionary Distance, and Maximum Parsimony Methods. Molecular biology and evolution. 2011;28(10):2731-9. doi: 10.1093/molbev/msr121.
81. Letunic I, Bork P. Interactive Tree Of Life v2: online annotation and display of phylogenetic trees made easy. Nucleic acids research. 2011;39(Web Server

issue):W475-8. Epub 2011/04/08. doi: 10.1093/nar/gkr201. PubMed PMID: 21470960; PubMed Central PMCID: PMC3125724.

82. Hampl V, Hug L, Leigh JW, Dacks JB, Lang BF, Simpson AG, et al. Phylogenomic analyses support the monophyly of Excavata and resolve relationships among eukaryotic "supergroups". Proc Natl Acad Sci U S A. 2009;106(10):3859-64. Epub 2009/02/25. doi: 10.1073/pnas.0807880106. PubMed PMID: 19237557; PubMed Central PMCID: PMC2656170.

83. Krogh A, Larsson B, von Heijne G, Sonnhammer EL. Predicting transmembrane protein topology with a hidden Markov model: application to complete genomes. Journal of molecular biology. 2001;305(3):567-80. Epub 2001/01/12. doi: 10.1006/jmbi.2000.4315. PubMed PMID: 11152613.

84. Lupas A, Van Dyke M, Stock J. Predicting coiled coils from protein sequences. Science. 1991;252(5010):1162-4. Epub 1991/05/24. PubMed PMID: 2031185.

85. Claros MG, Vincens P. Computational method to predict mitochondrially imported proteins and their targeting sequences. European journal of biochemistry / FEBS. 1996;241(3):779-86. Epub 1996/11/01. PubMed PMID: 8944766.

86. Haft DH, Selengut JD, White O. The TIGRFAMs database of protein families. Nucleic acids research. 2003;31(1):371-3. Epub 2003/01/10. PubMed PMID: 12520025; PubMed Central PMCID: PMCPmc165575.

87. Lim CC, Apstein CS, Colucci WS, Liao R. Impaired cell shortening and relengthening with increased pacing frequency are intrinsic to the senescent mouse cardiomyocyte. J Mol Cell Cardiol. 2000;32(11):2075-82. doi: 10.1006/jmcc.2000.1239. PubMed PMID: 11040110.

88. Nagata K, Liao R, Eberli FR, Satoh N, Chevalier B, Apstein CS, et al. Early changes in excitation-contraction coupling: transition from compensated hypertrophy to failure in Dahl salt-sensitive rat myocytes. Cardiovascular research. 1998;37(2):467-77. PubMed PMID: 9614501.

89. Zhan Y, Brown C, Maynard E, Anshelevich A, Ni W, Ho IC, et al. Ets-1 is a critical regulator of Ang II-mediated vascular inflammation and remodeling. Journal of Clinical Investigation. 2005;115(9):2508-16. doi: 10.1172/JCI24403. PubMed PMID: PMC1193876.

90. Chen P-C, Wakimoto H, Conner D, Araki T, Yuan T, Roberts A, et al. Activation of multiple signaling pathways causes developmental defects in mice with a Noonan syndrome–associated Sos1 mutation. The Journal of Clinical Investigation. 2010;120(12):4353-65. doi: 10.1172/JCI43910. PubMed PMID: PMC2993597.
91. Christodoulou DC, Gorham JM, Herman DS, Seidman JG. Construction of normalized RNA-seq libraries for next-generation sequencing using the crab duplex-specific nuclease. Current protocols in molecular biology / edited by Frederick M Ausubel [et al]. 2011;Chapter 4:Unit4 12. doi: 10.1002/0471142727.mb0412s94. PubMed PMID: 21472699; PubMed Central PMCID: PMC3152986.
92. Syed F. Application of Nextera[trade] technology to RNA-seq library preparation. Nat Meth. 2010;7(12).
93. Trapnell C, Roberts A, Goff L, Pertea G, Kim D, Kelley DR, et al. Differential gene and transcript expression analysis of RNA-seq experiments with TopHat and Cufflinks. Nature protocols. 2012;7(3):562-78. doi: 10.1038/nprot.2012.016. PubMed PMID: 22383036; PubMed Central PMCID: PMC3334321.
94. Christodoulou DC, Gorham JM, Kawana M, DePalma SR, Herman DS, Wakimoto H. Quantification of gene transcripts with deep sequencing analysis of gene expression (DSAGE) using 1 to 2 microg total RNA. Current protocols in molecular biology / edited by Frederick M Ausubel [et al]. 2011;Chapter 25:Unit25B 9. doi: 10.1002/0471142727.mb25b09s93. PubMed PMID: 21225638; PubMed Central PMCID: PMC4139004.
95. Trapnell C, Hendrickson DG, Sauvageau M, Goff L, Rinn JL, Pachter L. Differential analysis of gene regulation at transcript resolution with RNA-seq. Nat Biotech. 2013;31(1):46-53. doi: http://www.nature.com/nbt/journal/v31/n1/abs/nbt.2450.html#supplementary-information.
96. Burke MA, Chang S, Christodoulou DC, Gorham JM, Wakimoto H, Seidman CE, et al. Proliferation of Cardiac Fibroblasts Defines Early Stages of Genetic Dilated Cardiomyopathy and Precedes Myocardial Metabolic Derangement. Circulation Research. 2014;115(Suppl 1):A290.

97. Huang da W, Sherman BT, Lempicki RA. Systematic and integrative analysis of large gene lists using DAVID bioinformatics resources. Nature protocols. 2009;4(1):44-57. doi: 10.1038/nprot.2008.211. PubMed PMID: 19131956.
98. Wu AR, Neff NF, Kalisky T, Dalerba P, Treutlein B, Rothenberg ME, et al. Quantitative assessment of single-cell RNA-sequencing methods. Nature methods. 2014;11(1):41-6.
99. Schmitt JP, Kamisago M, Asahi M, Li GH, Ahmad F, Mende U, et al. Dilated cardiomyopathy and heart failure caused by a mutation in phospholamban. Science. 2003;299(5611):1410-3.
100. Geisterfer-Lowrance AA, Christe M, Conner DA, Ingwall JS, Schoen FJ, Seidman CE, et al. A mouse model of familial hypertrophic cardiomyopathy. Science. 1996;272(5262):731-4.
101. Santulli G, Xie W, Reiken SR, Marks AR. Mitochondrial calcium overload is a key determinant in heart failure. Proceedings of the National Academy of Sciences. 2015;112(36):11389-94.
102. Gorski Przemek A, Ceholski Delaine K, Hajjar Roger J. Altered Myocardial Calcium Cycling and Energetics in Heart Failure—A Rational Approach for Disease Treatment. Cell Metabolism. 2015;21(2):183-94. doi: http://dx.doi.org/10.1016/j.cmet.2015.01.005.
103. Semsarian C, Ahmad I, Giewat M, Georgakopoulos D, Schmitt JP, McConnell BK, et al. The L-type calcium channel inhibitor diltiazem prevents cardiomyopathy in a mouse model. J Clin Invest. 2002;109(8):1013-20. Epub 2002/04/17. doi: 10.1172/jci14677. PubMed PMID: 11956238; PubMed Central PMCID: PMCPmc150949.
104. Nagueh SF, Appleton CP, Gillebert TC, Marino PN, Oh JK, Smiseth OA, et al. Recommendations for the evaluation of left ventricular diastolic function by echocardiography. Journal of the American Society of Echocardiography. 2009;22(2):107-33.
105. Tsang TS, Barnes ME, Gersh BJ, Bailey KR, Seward JB. Left atrial volume as a morphophysiologic expression of left ventricular diastolic dysfunction and relation to cardiovascular risk burden. The American journal of cardiology. 2002;90(12):1284-9.

106. Foster LJ, de Hoog CL, Zhang Y, Zhang Y, Xie X, Mootha VK, et al. A mammalian organelle map by protein correlation profiling. Cell. 2006;125(1):187-99. doi: 10.1016/j.cell.2006.03.022. PubMed PMID: 16615899.
107. Crowley SD, Gurley SB, Herrera MJ, Ruiz P, Griffiths R, Kumar AP, et al. Angiotensin II causes hypertension and cardiac hypertrophy through its receptors in the kidney. Proceedings of the National Academy of Sciences of the United States of America. 2006;103(47):17985-90. doi: 10.1073/pnas.0605545103. PubMed PMID: PMC1693859.
108. Sun X, Iida S, Yoshikawa A, Senbonmatsu R, Imanaka K, Maruyama K, et al. Non-activated APJ suppresses the angiotensin II type 1 receptor, whereas apelin-activated APJ acts conversely. Hypertension research : official journal of the Japanese Society of Hypertension. 2011;34(6):701-6. Epub 2011/03/18. doi: 10.1038/hr.2011.19. PubMed PMID: 21412239.
109. Siddiquee K, Hampton J, McAnally D, May L, Smith L. The apelin receptor inhibits the angiotensin II type 1 receptor via allosteric trans-inhibition. British journal of pharmacology. 2013;168(5):1104-17. Epub 2012/09/01. doi: 10.1111/j.1476-5381.2012.02192.x. PubMed PMID: 22935142; PubMed Central PMCID: PMCPmc3594671.
110. Huggins GS, Lepore JJ, Greytak S, Patten R, McNamee R, Aronovitz M, et al. The CREB leucine zipper regulates CREB phosphorylation, cardiomyopathy, and lethality in a transgenic model of heart failure2007 2007-09-01 00:00:00. H1877-H82 p.
111. Fentzke RC, Korcarz CE, Lang RM, Lin H, Leiden JM. Dilated cardiomyopathy in transgenic mice expressing a dominant-negative CREB transcription factor in the heart. Journal of Clinical Investigation. 1998;101(11):2415-26. PubMed PMID: PMC508831.
112. Fentzke RC, Korcarz CE, Lang RM, Lin H, Leiden JM. Dilated cardiomyopathy in transgenic mice expressing a dominant-negative CREB transcription factor in the heart. Journal of Clinical Investigation. 1998;101(11):2415.
113. Gaasch WH, Zile MR. Left Ventricular Diastolic Dysfunction and Diastolic Heart Failure. Annual Review of Medicine. 2004;55(1):373-94. doi: 10.1146/annurev.med.55.091902.104417.

114. Kass DA, Bronzwaer JG, Paulus WJ. What mechanisms underlie diastolic dysfunction in heart failure? Circulation research. 2004;94(12):1533-42.
115. Hasenfuss G, Pieske B. Calcium Cycling in Congestive Heart Failure. Journal of Molecular and Cellular Cardiology. 2002;34(8):951-69. doi: http://dx.doi.org/10.1006/jmcc.2002.2037.
116. del Monte F, Harding SE, Dec GW, Gwathmey JK, Hajjar RJ. Targeting phospholamban by gene transfer in human heart failure. Circulation. 2002;105(8):904-7.
117. O'Rourke B, Kass DA, Tomaselli GF, Kääb S, Tunin R, Marbán E. Mechanisms of altered excitation-contraction coupling in canine tachycardia-induced heart failure, I experimental studies. Circulation research. 1999;84(5):562-70.
118. Schmidt U, Hajjar RJ, Helm PA, Kim CS, Doye AA, Gwathmey JK. Contribution of Abnormal Sarcoplasmic Reticulum ATPase Activity to Systolic and Diastolic Dysfunction in Human Heart Failure. Journal of Molecular and Cellular Cardiology. 1998;30(10):1929-37. doi: http://dx.doi.org/10.1006/jmcc.1998.0748.
119. Williams GS, Boyman L, Chikando AC, Khairallah RJ, Lederer W. Mitochondrial calcium uptake. Proceedings of the National Academy of Sciences. 2013;110(26):10479-86.
120. Freestone T, Turner RJ, Coady A, Higman DJ, Greenhalgh RM, Powell JT. Inflammation and Matrix Metalloproteinases in the Enlarging Abdominal Aortic Aneurysm. Arteriosclerosis, Thrombosis, and Vascular Biology. 1995;15(8):1145-51. doi: 10.1161/01.atv.15.8.1145.
121. Newman KM, Ogata Y, Malon AM, Irizarry E, Gandhi RH, Nagase H, et al. Identification of matrix metalloproteinases 3 (stromelysin-1) and 9 (gelatinase B) in abdominal aortic aneurysm. Arteriosclerosis, Thrombosis, and Vascular Biology. 1994;14(8):1315-20. doi: 10.1161/01.atv.14.8.1315.
122. Ramos-Mozo P, Rodriguez C, Pastor-Vargas C, Blanco-Colio LM, Martinez-Gonzalez J, Meilhac O, et al. Plasma profiling by a protein array approach identifies IGFBP-1 as a novel biomarker of abdominal aortic aneurysm. Atherosclerosis. 2012;221(2):544-50. doi: http://dx.doi.org/10.1016/j.atherosclerosis.2012.01.009.
123. Sukhanov S, Higashi Y, Shai S-Y, Vaughn C, Mohler J, Li Y, et al. IGF-1 Reduces Inflammatory Responses, Suppresses Oxidative Stress, and Decreases

Atherosclerosis Progression in ApoE-Deficient Mice. Arteriosclerosis, Thrombosis, and Vascular Biology. 2007;27(12):2684-90. doi: 10.1161/atvbaha.107.156257.
124. Shimizu K, Mitchell RN, Libby P. Inflammation and Cellular Immune Responses in Abdominal Aortic Aneurysms. Arteriosclerosis, Thrombosis, and Vascular Biology. 2006;26(5):987-94. doi: 10.1161/01.ATV.0000214999.12921.4f.
125. Saracini C, Bolli P, Sticchi E, Pratesi G, Pulli R, Sofi F, et al. Polymorphisms of genes involved in extracellular matrix remodeling and abdominal aortic aneurysm. Journal of vascular surgery. 2012;55(1):171-9.e2. Epub 2011/11/19. doi: 10.1016/j.jvs.2011.07.051. PubMed PMID: 22094117.
126. Morris DR, Biros E, Cronin O, Kuivaniemi H, Golledge J. The association of genetic variants of matrix metalloproteinases with abdominal aortic aneurysm: a systematic review and meta-analysis. Heart (British Cardiac Society). 2014;100(4):295-302. Epub 2013/07/03. doi: 10.1136/heartjnl-2013-304129. PubMed PMID: 23813847.
127. Silence J, Lupu F, Collen D, Lijnen HR. Persistence of Atherosclerotic Plaque but Reduced Aneurysm Formation in Mice With Stromelysin-1 (MMP-3) Gene Inactivation. Arteriosclerosis, Thrombosis, and Vascular Biology. 2001;21(9):1440-5. doi: 10.1161/hq0901.097004.
128. Superti-Furga A, Gugler E, Gitzelmann R, Steinmann B. Ehlers-Danlos syndrome type IV: a multi-exon deletion in one of the two COL3A1 alleles affecting structure, stability, and processing of type III procollagen. The Journal of biological chemistry. 1988;263(13):6226-32. Epub 1988/05/05. PubMed PMID: 2834369.
129. Vissing H, D'Alessio M, Lee B, Ramirez F, Byers PH, Steinmann B, et al. Multiexon deletion in the procollagen III gene is associated with mild Ehlers-Danlos syndrome type IV. The Journal of biological chemistry. 1991;266(8):5244-8. Epub 1991/03/15. PubMed PMID: 2002056.
130. Sasaki T, Arai K, Ono M, Yamaguchi T, Furuta S, Nagai Y. Ehlers-Danlos syndrome. A variant characterized by the deficiency of pro alpha 2 chain of type I procollagen. Archives of dermatology. 1987;123(1):76-9. Epub 1987/01/01. PubMed PMID: 3800425.

131. Milewicz DM, Michael K, Fisher N, Coselli JS, Markello T, Biddinger A. Fibrillin-1 (FBN1) mutations in patients with thoracic aortic aneurysms. Circulation. 1996;94(11):2708-11.
132. Boileau C, Guo D-C, Hanna N, Regalado ES, Detaint D, Gong L, et al. TGFB2 loss of function mutations cause familial thoracic aortic aneurysms and acute aortic dissections associated with mild systemic features of the Marfan syndrome. Nature genetics. 2012;44(8):916.
133. Lerner-Ellis JP, Aldubayan SH, Hernandez AL, Kelly MA, Stuenkel AJ, Walsh J, et al. The spectrum of FBN1, TGFβR1, TGFβR2 and ACTA2 variants in 594 individuals with suspected Marfan Syndrome, Loeys–Dietz Syndrome or Thoracic Aortic Aneurysms and Dissections (TAAD). Molecular genetics and metabolism. 2014;112(2):171-6.
134. Ang LS, Boivin WA, Williams SJ, Zhao H, Abraham T, Carmine-Simmen K, et al. Serpina3n attenuates granzyme B-mediated decorin cleavage and rupture in a murine model of aortic aneurysm. Cell death & disease. 2011;2:e209. Epub 2011/09/09. doi: 10.1038/cddis.2011.88. PubMed PMID: 21900960; PubMed Central PMCID: PMCPmc3186906.
135. Liu Z, Morgan S, Ren J, Wang Q, Annis DS, Mosher DF, et al. Thrombospondin-1 (TSP1) Contributes to the Development of Vascular Inflammation by Regulating Monocytic Cell Motility in Mouse Models of Abdominal Aortic Aneurysm. Circulation Research. 2015;117(2):129-41. doi: 10.1161/circresaha.117.305262.
136. Chandesris MO, Azarine A, Ong KT, Taleb S, Boutouyrie P, Mousseaux E, et al. Frequent and widespread vascular abnormalities in human signal transducer and activator of transcription 3 deficiency. Circulation Cardiovascular genetics. 2012;5(1):25-34. Epub 2011/11/16. doi: 10.1161/circgenetics.111.961235. PubMed PMID: 22084479.
137. Obama T, Tsuji T, Kobayashi T, Fukuda Y, Takayanagi T, Taro Y, et al. Epidermal growth factor receptor inhibitor protects against abdominal aortic aneurysm in a mouse model. Clinical science (London, England : 1979). 2015;128(9):559-65. Epub 2014/12/23. doi: 10.1042/cs20140696. PubMed PMID: 25531554.

138. Hofmann MA, Drury S, Fu C, Qu W, Taguchi A, Lu Y, et al. RAGE mediates a novel proinflammatory axis: a central cell surface receptor for S100/calgranulin polypeptides. Cell. 1999;97(7):889-901. Epub 1999/07/10. PubMed PMID: 10399917.
139. Hofmann Bowman M, Wilk J, Heydemann A, Kim G, Rehman J, Lodato JA, et al. S100A12 mediates aortic wall remodeling and aortic aneurysm. Circulation research. 2010;106(1):145-54. doi: 10.1161/CIRCRESAHA.109.209486. PubMed PMID: PMC2878187.
140. Averill MM, Kerkhoff C, Bornfeldt KE. S100A8 and S100A9 in Cardiovascular Biology and Disease. Arteriosclerosis, Thrombosis, and Vascular Biology. 2012;32(2):223-9. doi: 10.1161/atvbaha.111.236927.
141. Cao J, Geng L, Wu Q, Wang W, Chen Q, Lu L, et al. Spatiotemporal expression of matrix metalloproteinases (MMPs) is regulated by the Ca2+-signal transducer S100A4 in the pathogenesis of thoracic aortic aneurysm. PloS one. 2013;8(7):e70057. Epub 2013/08/08. doi: 10.1371/journal.pone.0070057. PubMed PMID: 23922901; PubMed Central PMCID: PMCPmc3726393.
142. Coen M, Burkhardt K, Bijlenga P, Gabbiani G, Schaller K, Kovari E, et al. Smooth muscle cells of human intracranial aneurysms assume phenotypic features similar to those of the atherosclerotic plaque. Cardiovascular pathology : the official journal of the Society for Cardiovascular Pathology. 2013;22(5):339-44. Epub 2013/03/08. doi: 10.1016/j.carpath.2013.01.083. PubMed PMID: 23466011.
143. Shah BH, Catt KJ. Calcium-Independent Activation of Extracellularly Regulated Kinases 1 and 2 by Angiotensin II in Hepatic C9 Cells: Roles of Protein Kinase Cδ, Src/Proline-Rich Tyrosine Kinase 2, and Epidermal Growth Factor Receptor trans-Activation. Molecular Pharmacology. 2002;61(2):343-51. doi: 10.1124/mol.61.2.343.
144. Olson ER, Shamhart PE, Naugle JE, Meszaros JG. Angiotensin II-Induced Extracellular Signal-Regulated Kinase 1/2 Activation Is Mediated by Protein Kinase Cδ and Intracellular Calcium in Adult Rat Cardiac Fibroblasts. Hypertension. 2008;51(3):704-11. doi: 10.1161/hypertensionaha.107.098459.
145. Regalado ES, Guo D-c, Villamizar C, Avidan N, Gilchrist D, McGillivray B, et al. Exome sequencing identifies SMAD3 mutations as a cause of familial thoracic aortic

aneurysm and dissection with intracranial and other arterial aneurysms. Circulation research. 2011;109(6):680-6.
146. Doyle JJ, Doyle AJ, Wilson NK, Habashi JP, Bedja D, Whitworth RE, et al. A deleterious gene-by-environment interaction imposed by calcium channel blockers in Marfan syndrome. eLife. 2015;4. doi: 10.7554/eLife.08648.
147. Wilmink AB, Vardulaki KA, Hubbard CS, Day NE, Ashton HA, Scott AP, et al. Are antihypertensive drugs associated with abdominal aortic aneurysms? Journal of vascular surgery. 2002;36(4):751-7. PubMed PMID: 12368736.
148. Doughan AK, Harrison DG, Dikalov SI. Molecular Mechanisms of Angiotensin II–Mediated Mitochondrial Dysfunction: Linking Mitochondrial Oxidative Damage and Vascular Endothelial Dysfunction. Circulation Research. 2008;102(4):488-96. doi: 10.1161/circresaha.107.162800.
149. Daugherty A, Cassis LA. Mouse models of abdominal aortic aneurysms. Arteriosclerosis, thrombosis, and vascular biology. 2004;24(3):429-34.
150. Kuhlencordt PJ, Gyurko R, Han F, Scherrer-Crosbie M, Aretz TH, Hajjar R, et al. Accelerated atherosclerosis, aortic aneurysm formation, and ischemic heart disease in apolipoprotein E/endothelial nitric oxide synthase double-knockout mice. Circulation. 2001;104(4):448-54.
151. Hoffman NE, Chandramoorthy HC, Shamugapriya S, Zhang X, Rajan S, Mallilankaraman K, et al. MICU1 Motifs Define Mitochondrial Calcium Uniporter Binding and Activity. Cell Rep. 2013;5(6):1576-88. doi: 10.1016/j.celrep.2013.11.026. PubMed PMID: 24332854; PubMed Central PMCID: PMCPmc3919628.

Figures and Tables

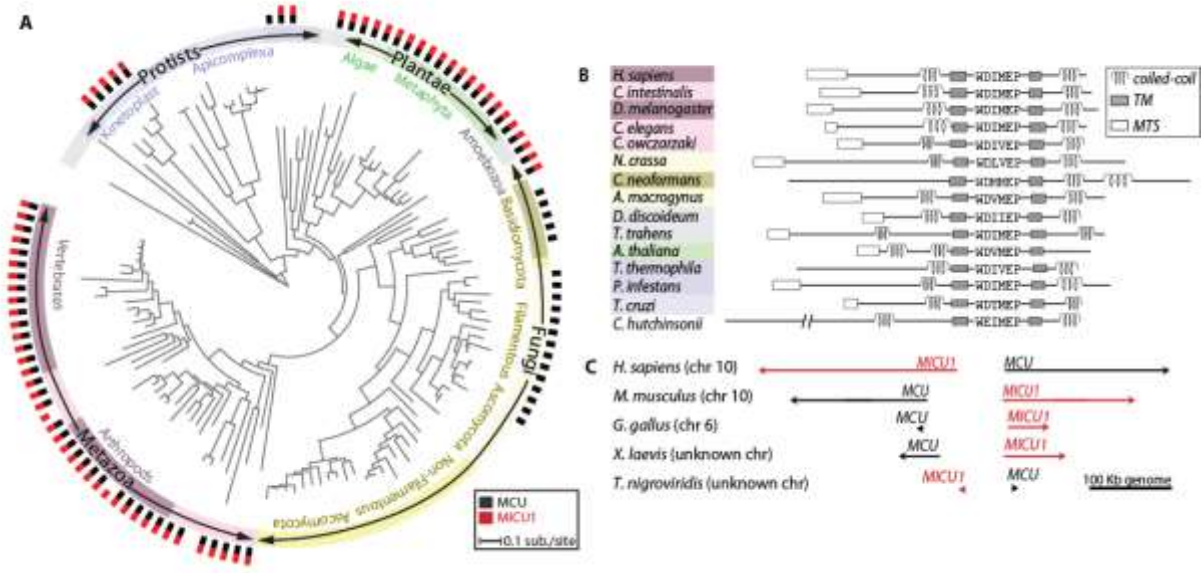

Figure 1. **(A)** Eukaryotic tree of life annotated with presence of *MCU* (black) and *MICU1* (red) homologs, detailed version available in Figure 2. **(B)** Protein domain architecture of MCU homologs, including mitochondrial targeting sequence (white rectangle), coiled-coil domain (coil), transmembrane domain (shaded rectangle), and the DIME motif. **(C)** Genomic organization of *MICU1* and *MCU* across vertebrate genomes.

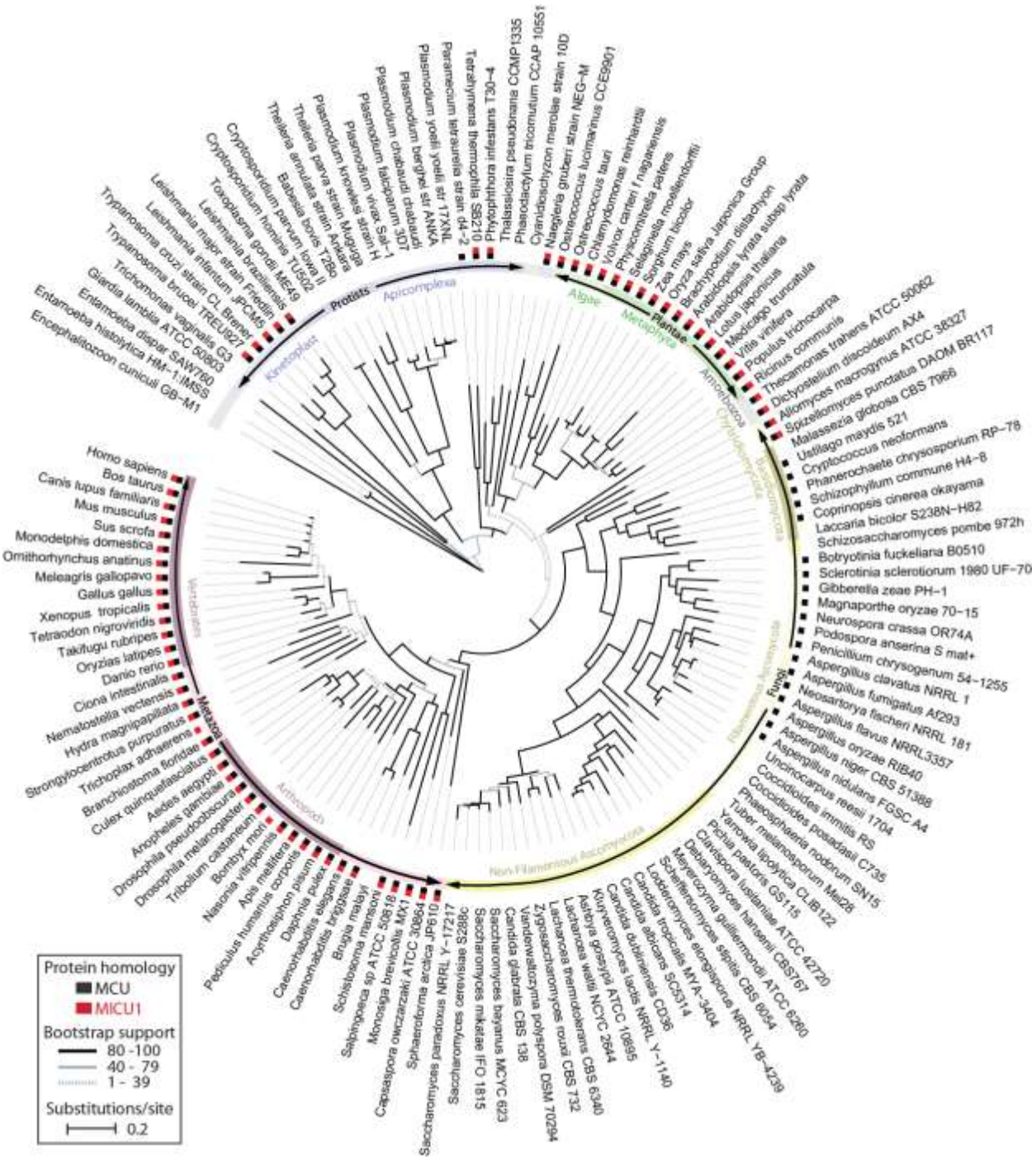

Figure 2. Eukaryotic tree of life annotated with *MCU* (black) and *MICU1* (red) homologs.

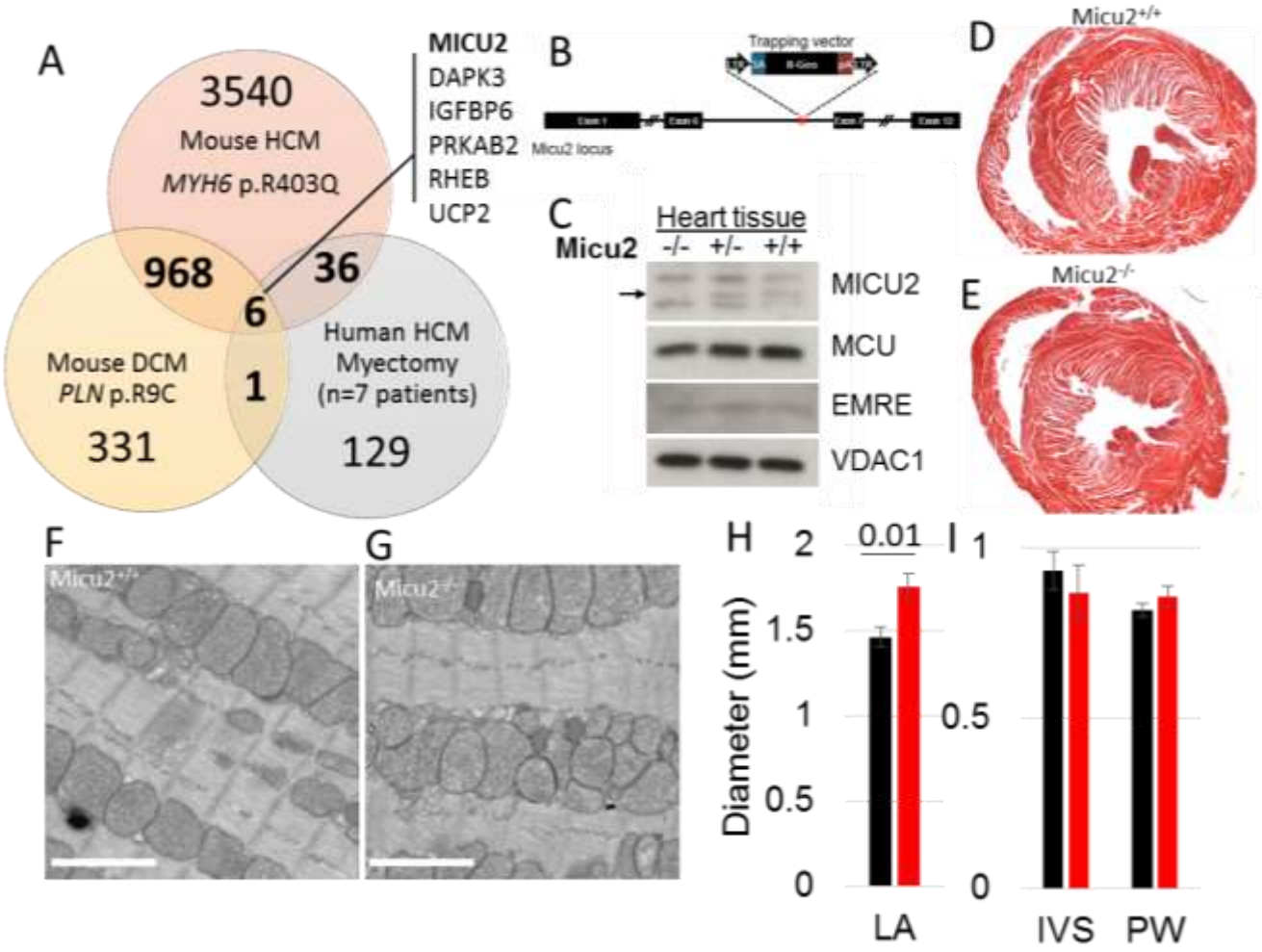

Figure 3. Integrative analysis of transcriptome datasets and characterization of the *Micu2*$^{-/-}$ mouse hearts. (**A**) Integration of RNA-seq profiles from human and mouse cardiomyopathy. Intersecting seven human HCM patient cardiac muscle transcriptomes with mouse models of hypertrophic cardiomyopathy (HCM) and dilated cardiomyopathy (DCM) identified 6 consistently differentially expressed genes including mitochondrial calcium uniporter component *Micu2*. (**B**) Schema of *Micu2* gene trap vector used to generate the *Micu2*$^{-/-}$ mouse. (**C**) Protein levels of the mitochondrial calcium uniporter regulatory component *Micu2* were significantly reduced in *Micu2*$^{-/-}$ mouse hearts. Uniporter core calcium channel *Mcu* had ~30% decreased protein expression. (**D** and **E**). Hearts of *Micu2*$^{-/-}$ mice were histologically indistinguishable from wildtype littermates. (**F** and **G**) Representative electron microscopy sections of Micu2$^{-/-}$ and wildtype mouse hearts. Scale bar: 10 um. H-I. Longitudinal evaluation by echocardiography identified

increased left atrial (LA) size consistent with diastolic dysfunction but no significant differences in interventricular septum (IVS), posterior wall (PW) thickness.

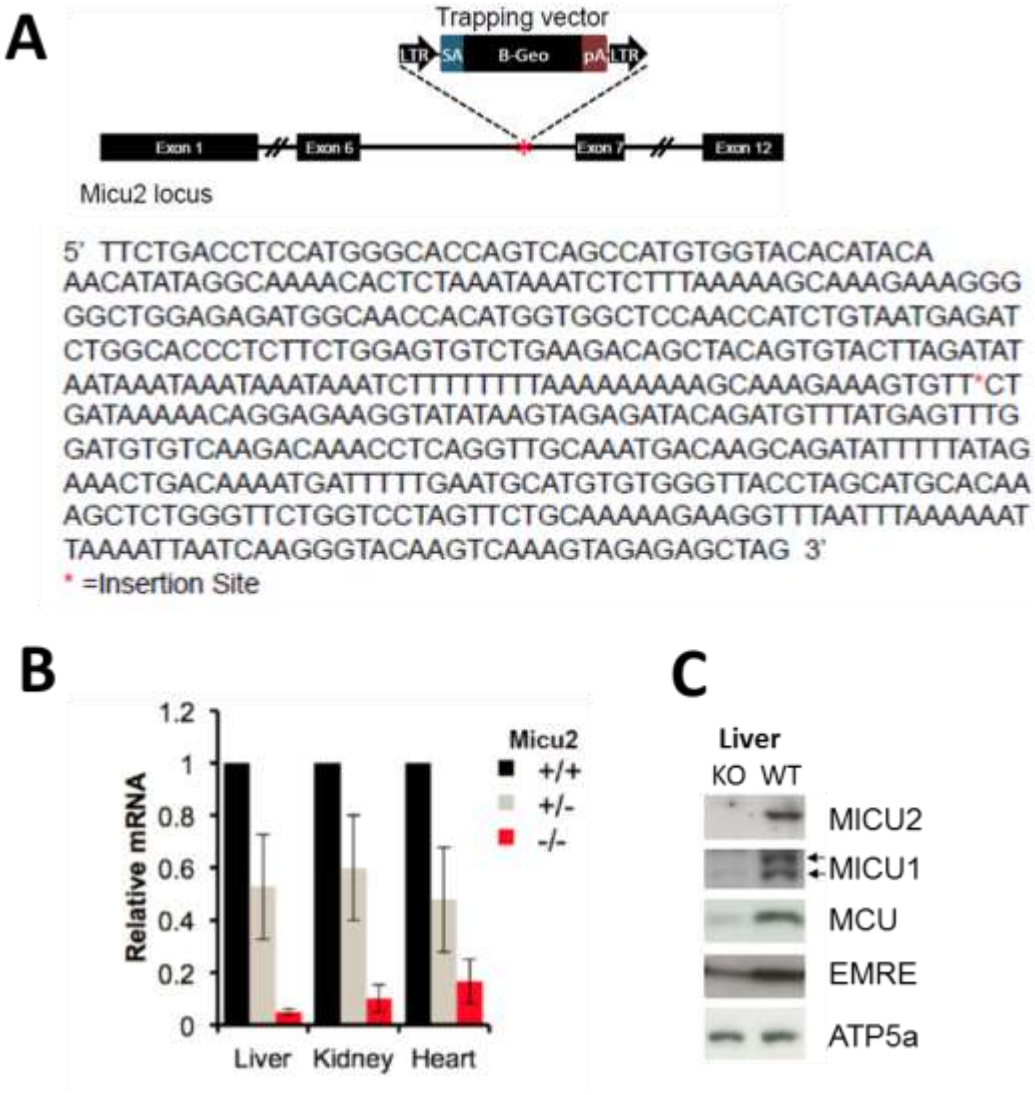

Figure 4. Gene trap disruption of *Micu2* locus. (**A**) Schematic showing the mouse Micu2 genomic locus, highlighting where the gene trapping vector is inserted. The gene trap vector (VICTR 37) has a β-Geo selection marker, along with a splice acceptor (SA) and transcription termination sequence (pA) and is flanked by retroviral long terminal repeat sequences. The genomic DNA sequence surrounding the gene trap vector insertion site is shown. The insertion site is indicated with a red asterisk. (**B**) *Micu2*$^{+/-}$ mice had a 50% reduction in Micu2 expression across liver, kidney and heart by qPCR. *Micu2*$^{-/-}$ mice had further reduced levels of Micu2 expression. (**C**) Protein levels of the mitochondrial calcium uniporter complex components *MICU2*, *MICU1* and *MCU* were all significantly reduced in *Micu2*$^{-/-}$ mouse liver tissue.

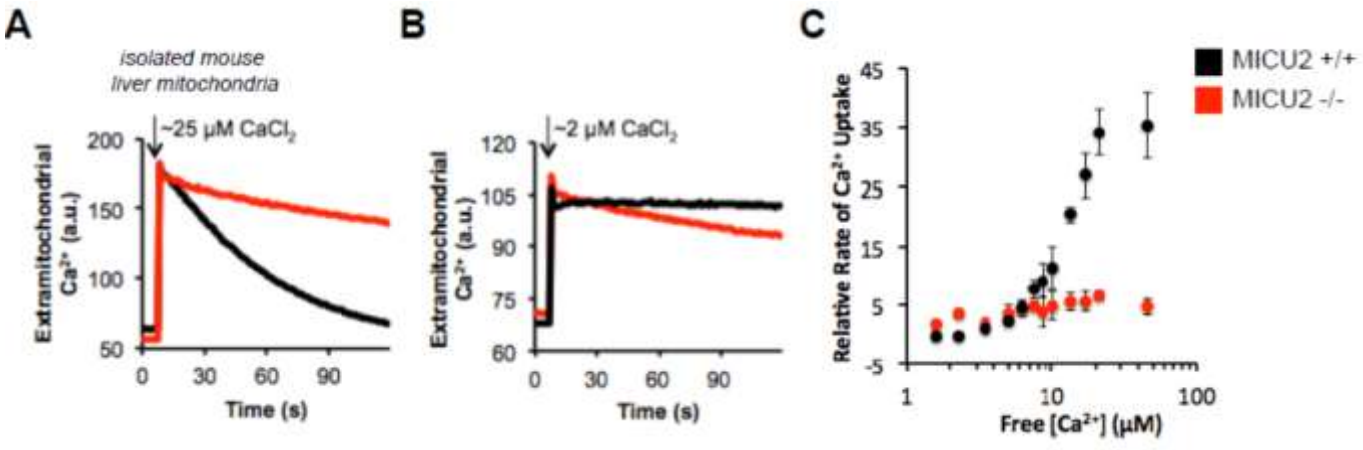

<u>Figure 5.</u> ***Micu2*$^{-/-}$ mouse liver mitochondria take up Ca^{2+} slower at high [Ca^{2+}] and faster at low [Ca^{2+}].** (**A** and **B**). Isolated mouse liver mitochondria were given a pulse of (**A**) ~25 μM or (**B**) ~2 μM $CaCl_2$. Extramitochondrial [Ca^{2+}] was measured using the membrane-impermeable calcium indicator Oregon Green BAPTA6F. (**C**) Relative rates of calcium uptake from experiments such as those in A and B at different injected [Ca^{2+}] in isolated mouse liver mitochondria (n=3).

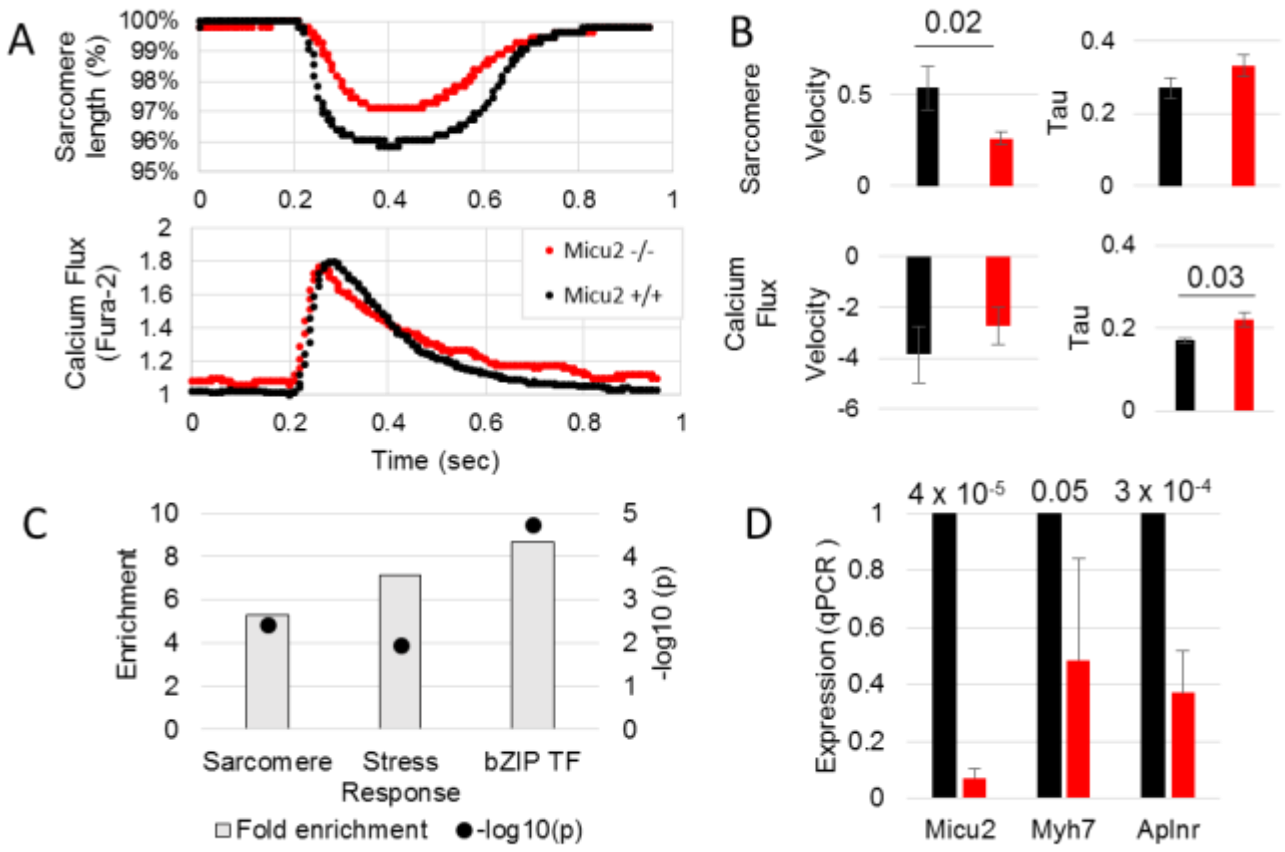

<u>Figure 6.</u> Functional, structural and transcriptional analysis of *Micu2*$^{-/-}$ cardiomyocytes. (**A**) Representative tracings of single myocyte sarcomere length (plotted as % of resting length) and calcium flux (plotted as normalized Fura-2 intensity) in *Micu2*$^{-/-}$ mice and wildtype littermates. (**B**) Micu2$^{-/-}$ cardiomyocytes had slower repolarization kinetics as evidenced by both decreased sarcomere relaxation velocity and increased time constant (Tau) for calcium reuptake compared to wildtype cardiomyocytes. (**C**) Transcriptome wide analysis of *Micu2*$^{-/-}$ and wildtype left ventricular tissue revealed enrichment in three gene sets: sarcomere components, stress response genes and bZip transcription factors. Plotted P-values are bonferoni-corrected. (**D**) *Micu2*, *Myh7* and *Aplnr* were three of the most differentially expressed genes in the left-ventricle RNA-seq datasets. Fold change differences in these genes were independently confirmed with quantitative-PCR in whole heart tissue from n=5 mice. Mean and standard deviation of *Micu2*$^{-/-}$ qPCR expression normalized to mean wildtype qPCR expression are plotted.

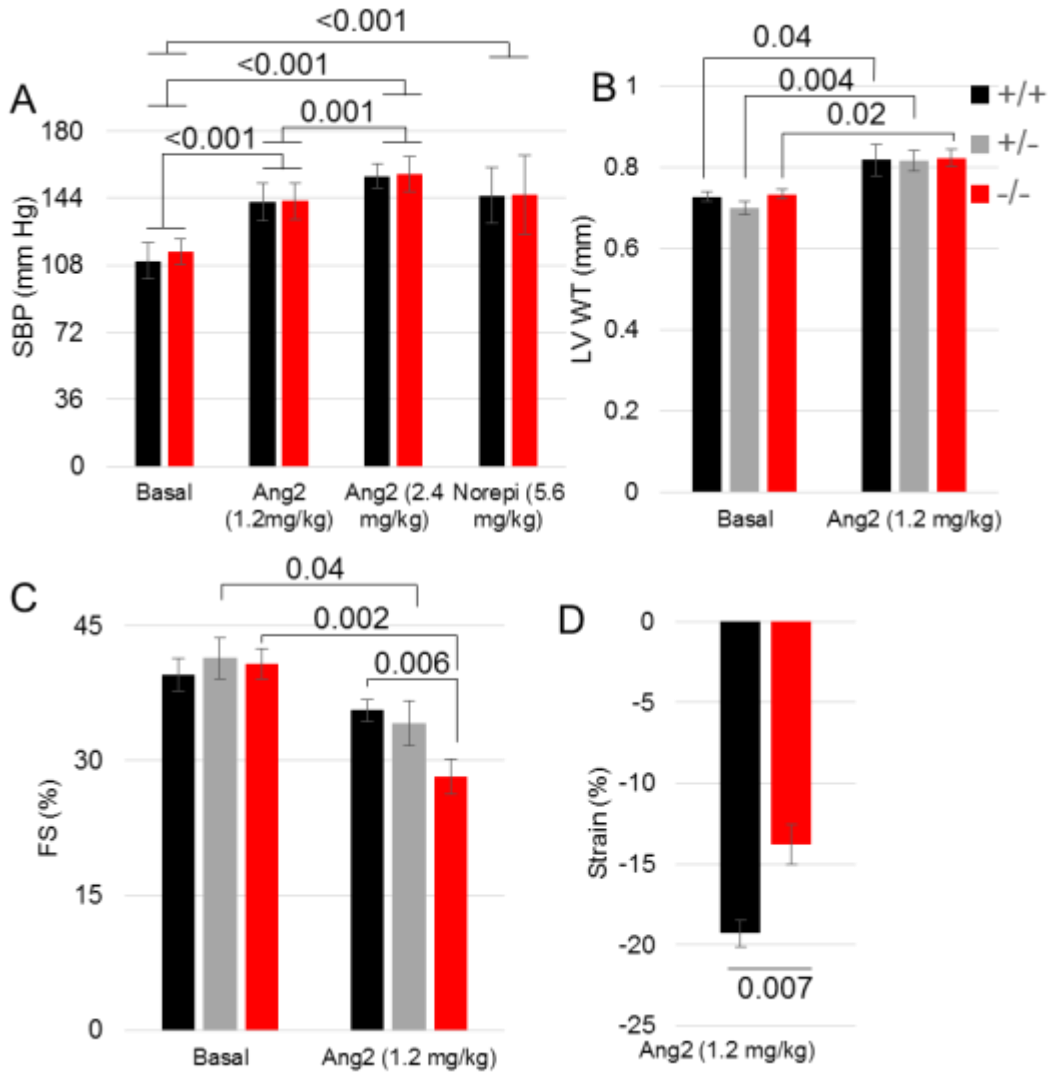

<u>Figure 7.</u> *Micu2*$^{-/-}$ mice have increased susceptibility to Angiotensin 2 mediated hypertensive dysfunction. (**A**) *Micu2*$^{-/-}$ and wildtype mice have equivalent systolic blood pressures at baseline and equivalently elevated pressures after angiotensin 2 infusion (1.2 mg/kg/day, 2.4 mg/kg/day) and norepinephrine infusion (5.6 mg/kg/day). (**B** and **C**) After 2 weeks of angiotensin 2 infusion, Micu2$^{-/-}$ mice have equivalent increases in left ventricular wall thickness (LV WT) in response to the hypertrophic stimuli, but have significantly worse systolic function as quantified by decrease in fractional shortening (FS). (**D**) Speckle tracking imaging analysis identifies decreased systolic tissue strain in Micu2$^{-/-}$ mice after two weeks of angiotensin 2 infusion consistent with systolic dysfunction. (*) $p<0.05$ (**) $p<0.01$, (***)$p<0.001$

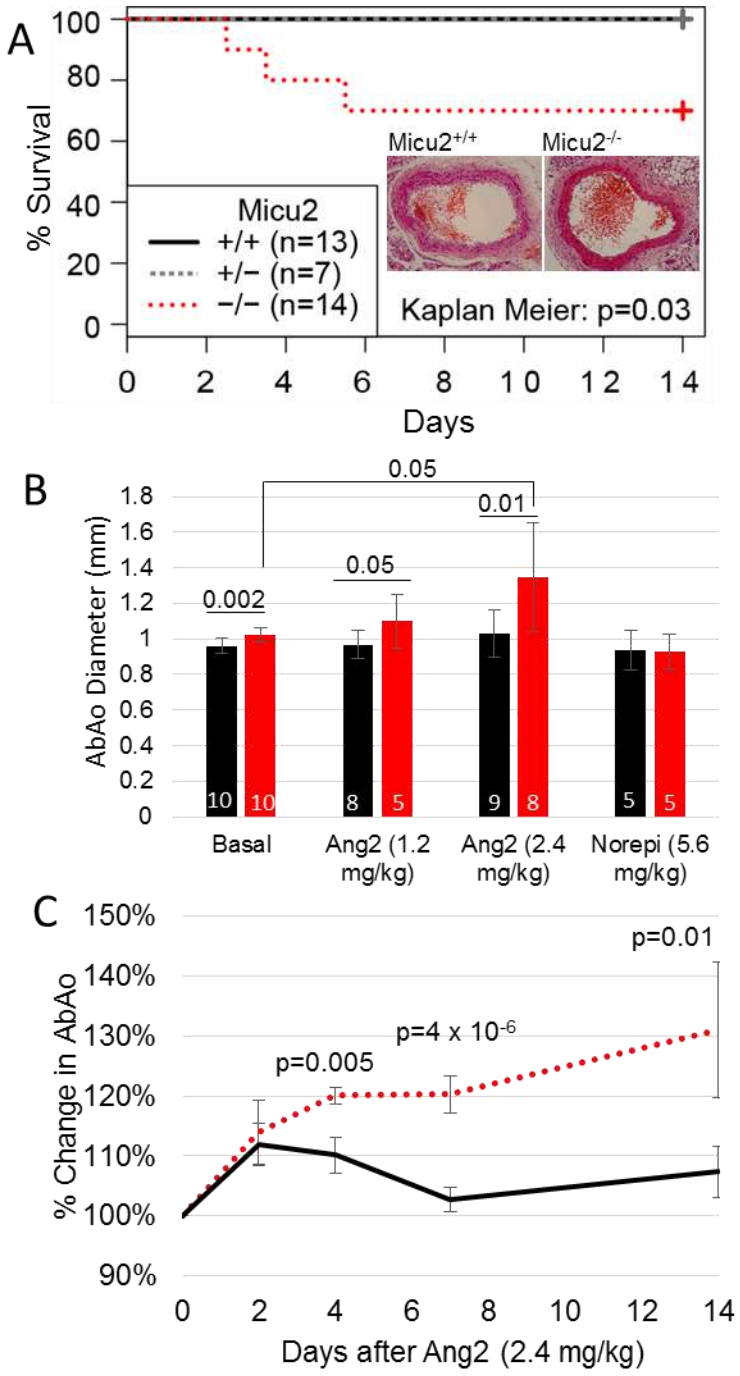

Figure 8. ***Micu2*$^{-/-}$ mice are susceptible to angiotensin 2 induced aortic aneurisms.** (**A**) *Micu2*$^{-/-}$ mice were observed to have an increased propensity to die from abdominal aortic aneurism rupture when stressed by angiotensin 2 (1.2 mg/kg, p=0.03). Inset: representative abdominal aorta histological sections after 2 weeks of angiotensin 2 infusion demonstrate grossly similar histologic patterns. (**B**) Abdominal Aortic diameter (AbAo) measured at baseline and 2 weeks after angiotensin 2 infusion identified slightly

enlarged aortic diameters of *Micu2*$^{-/-}$ mice at baseline that was greatly exaggerated with increasing angiotensin 2 dose (2.4 mg/kg). However, aorta diameter does not change in the presence of norepinephrine. (**C**) Serial measurements of abdominal aorta diameter in *Micu2*$^{-/-}$ and wildtype mice identified a differential aortic enlargement by day 4 of angiotensin 2 infusion (2.4 mg/kg). (*) $p<0.05$, (**) $p<0.01$

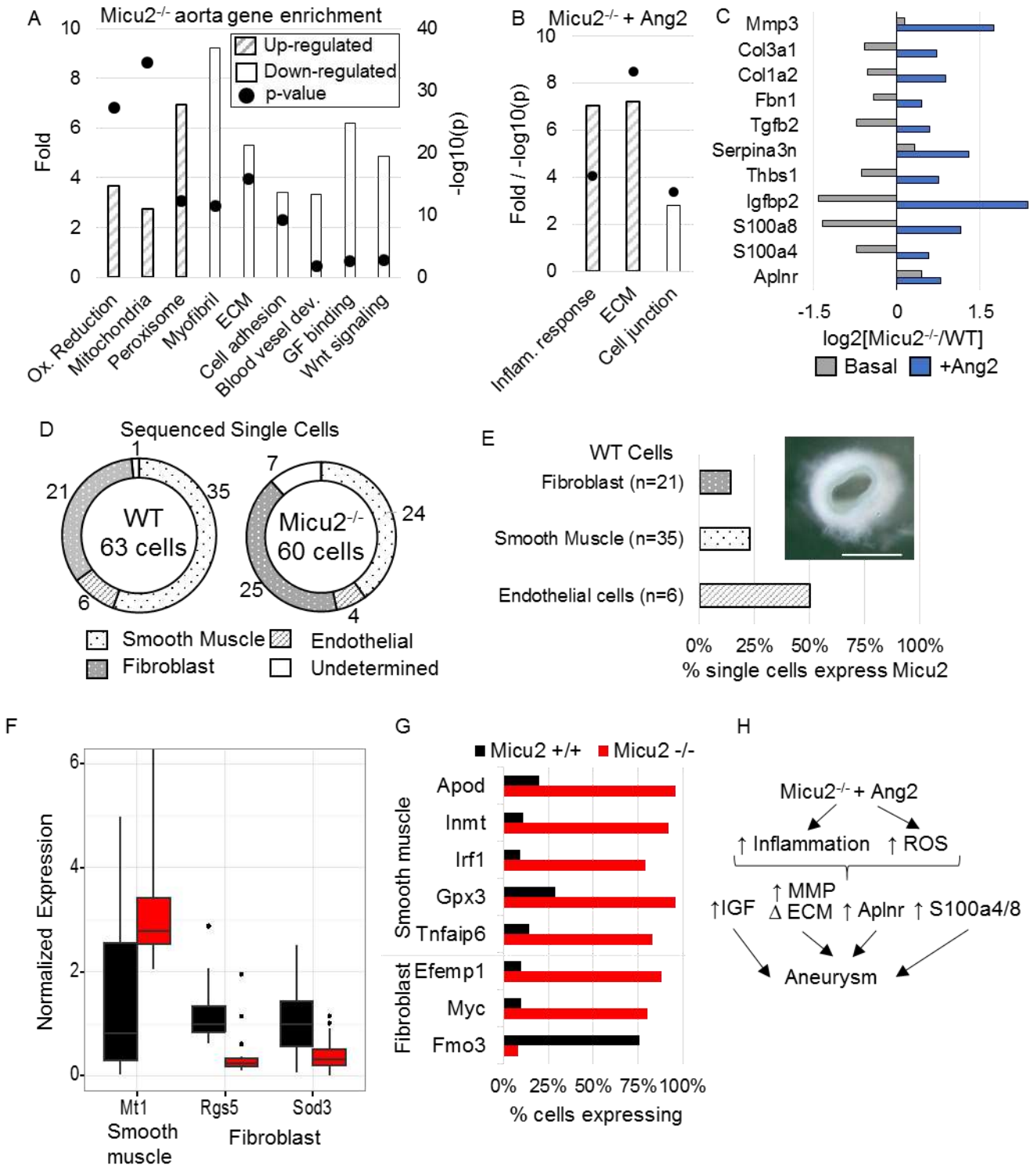

Figure 9. Transcriptional dissection of *Micu2*$^{-/-}$ aortic aneurysm. (**A**) RNA-seq pathway enrichment analysis of Micu2$^{-/-}$ gene expression compared to wildtype mice in the basal state without angiotensin infusion identifies numerous gene sets in genes that

are up-regulated (shaded bars) and down-regulated (unshaded bars). P-values are bonferoni corrected. (**B**) RNA-seq pathway enrichment analysis of mouse aorta tissue after 2 weeks of angiotensin 2 infusion (1.2 mg/kg) identified 3 notable expressed gene sets: an upregrulation of inflammatory response and ECM genes and a down-regulation of cell-junction genes. (**C**) Fold change of selected genes with known roles in aneyurism formation in the basal and Ang2 (1.2 mg/kg) state with significant differential expression by RNA-seq. (**D**) To elucidate early transcriptional changes leading to aneurysm formation, two mice were treated with high dose Angiotensin 2 (2.4 mg/kg) for 4 days. Aortas were dissected and captured on a microfluidic chip. Gene expression at the single cell level was analyzed. 63 cells from wildtype aortas and 60 cells from *Micu2*$^{-/-}$ aortas were available for analysis. The majority of single cells captured on the microfluidic chip were smooth muscle and fibroblast cells with a distinct minority of endothelial cells. This distribution was likely due to the size of the microfluidic chip. (**E**) In the wildtype mouse aorta single cells, *Micu2* was expressed in 50% of endothelial cells, 23% of smooth muscle cells and 14% of fibroblasts. Inset: LacZ staining of *Micu2*$^{+/-}$ mouse aorta reveals gross *Micu2* expression throughout the aorta suggesting that Micu2 expression is not limited to a single cell type. Scale bar is 500 um. (**F** and **G**) For smooth muscle and fibroblast cells, differences in level of gene expression were assessed with a Wilcox test and differences in the percent of cells expressing a transcript (defined as >5FPKM) was assessed with a Fisher test. Conservatively correcting for multiple hypothesis testing, 3 genes were differentially expressed in terms of level of expression (**F**) and 8 genes were differentially expressed in terms of percent of cells expression a transcript (**G**). The 11 genes were involved in cellular response to reactive oxygen species or cellular proliferation. (**H**) Transcriptional changes associated with Ang2 mediated abdominal aortic aneyurism formation in Micu2$^{-/-}$ mice. Single cell RNA-seq data identifies an inflammatory and ROS response at 4 days. Whole tissue RNA seq at 2 weeks identifies transcriptional upregulation of insulin growth factor (IGF) signaling, matrix metaloproteases (MMP), S100a4/8 and Aplnr as well as extracellular matrix (ECM) disregulation.

Table 1. Patient characteristics of myectomy samples used in bioinformatic screen.

Sample	Gender	Age at diagnosis	Age at myectomy	LV wall thickness (mm)	Genotype
1	Female	49	69	27	MYH7 p.A1051V
2	Female	45	52	18	MYH7 p.Y833H
3	Female	67	69	13	MYH7 p.G741R
4	Female	46	52	15	TNNT2 p.D81A
5	Female	26	45	18	Negative
6	Male	43	45	23	Negative
7	Male	31	31	32	Negative

Table 2. **Echocardiography of WT and MICU2$^{-/-}$ mice at 16-18 weeks.**

	WT (N=5)	MICU2$^{-/-}$ (N=6)	P
Age	16.97 (1.1)	16.92 (0.54)	0.94
Weight	43.66 (8.64)	36.08 (6.61)	0.15
Interventricular Septum (Mm)	0.93 (0.05)	0.87 (0.07)	0.11
Left Ventricular Diastolic Diameter (Mm)	3.32 (0.4)	3.48 (0.41)	0.53
Left Ventricular Posterior Wall (Mm)	0.82 (0.09)	0.85 (0.04)	0.43
Fractional Shortening (%)	48.6 (9.2)	48.4 (5.7)	0.97
Left Atrial Diameter (Mm)	1.5 (0.1)	1.8 (0.2)	0.01

Table 3. Single myocyte sarcomere transient measurements.

	WT (n=34 cells)	MICU2$^{-/-}$ (n=22 cells)	p
∆ sarcomere length (%)	4.14 (1.95)	3.81 (2.11)	0.28
Depolarization velocity	-1.09 (0.71)	-0.86 (0.54)	0.1
Repolarization velocity	0.54 (0.69)	0.26 (0.17)	**0.02**
Repolarization time constant (Tau)	0.27 (0.17)	0.33 (0.14)	0.06

Table 4. Single myocyte calcium transient measurements.

	WT (n=31 cells)	MICU2$^{-/-}$ (n=22 cells)	p
Total calcium flux	0.08 (0.04)	0.08 (0.03)	0.4
Depolarization velocity	22.79 (23.38)	29.24 (34.19)	0.21
Repolarization velocity	-3.85 (6.17)	-2.74 (3.45)	0.22
Repolarization time constant (Tau)	0.17 (0.04)	0.22 (0.08)	**0.03**

Table 5. Aorta diameter time course after Ang 2 (2.4 mg/kg).

	WT			MICU2-/-			P
DAY	N	Mean (mm)	Std. dev.	N	Mean (mm)	Std. dev	
0	5	0.971	0.033	5	1.022	0.032	0.042
2	5	1.087	0.077	5	1.163	0.114	0.26
4	5	1.069	0.070	5	1.227	0.030	0.0048
7	10	0.985	0.068	8	1.233	0.085	3.81E-06
14	9	1.029	0.130	8	1.344	0.307	0.024